JVST A
Journal of Vacuum Science & Technology A

PERSPECTIVE

avs.scitation.org/journal/jva

Conversion reactions in atomic layer processing with emphasis on ZnO conversion to Al_2O_3 by trimethylaluminum

Cite as: J. Vac. Sci. Technol. A 39, 021001 (2021); doi: 10.1116/6.0000680
Submitted: 30 September 2020 · Accepted: 5 January 2021 ·
Published Online: 1 February 2021

Tyler J. Myers, Austin M. Cano, Diane K. Lancaster, Joel W. Clancey, and Steven M. George

AFFILIATIONS

Department of Chemistry, University of Colorado, Boulder, Colorado 80309

Note: This paper is part of the 2021 Special Topic Collection on Atomic Layer Deposition (ALD).

ABSTRACT

Atomic layer processing such as atomic layer deposition (ALD) and thermal atomic layer etching (ALE) is usually described in terms of sequential, self-limiting surface reactions. This picture for ALD and thermal ALE leaves out the possibility that the metal precursor in ALD and thermal ALE can also convert the surface material to another new material. This perspective introduces the previous evidence for conversion reactions in atomic layer processing based on a variety of studies, including Al_2O_3 ALD on ZnO, growth of Zn(O,S) alloys, "self-cleaning" of III-V semiconductor surfaces, and thermal ALE of ZnO and SiO_2. The paper then focuses on the reaction of $Al(CH_3)_3$ [trimethylaluminum (TMA)] on ZnO as a model conversion system. A variety of techniques are utilized to monitor ZnO conversion to Al_2O_3 using TMA at 150 °C. These techniques include FTIR spectroscopy, quadrupole mass spectrometry (QMS), x-ray reflectivity (XRR), gravimetric analysis, x-ray photoelectron spectroscopy (XPS), and quartz crystal microbalance (QCM) measurements. The various studies focus on ZnO conversion to Al_2O_3 for both hydroxyl-terminated and ethyl-terminated ZnO substrates. FTIR studies observed the conversion of ZnO to Al_2O_3 and provided evidence that the conversion is self-limiting at higher TMA exposures. QMS studies identified the volatile reaction products during the TMA reaction with ZnO as CH_4, C_2H_4, C_2H_6, and $Zn(CH_3)_2$. The CH_4 reaction product preceded the appearance of the $Zn(CH_3)_2$ reaction product. XRR investigations determined that the thickness of the Al_2O_3 conversion layer on ZnO limits at ~1.0 nm at 150 °C after larger TMA exposures. A gravimetric analysis of the conversion reaction on ZnO nanoparticles with a diameter of 10 nm displayed a percent mass loss of ~49%. This mass loss is consistent with an Al_2O_3 shell of ~1 nm on a ZnO core with a diameter of ~6 nm. XPS studies revealed that ZnO ALD films with a thickness of 2 nm were almost completely converted to Al_2O_3 by large TMA exposures at 150 °C. QCM investigations then measured the mass changes for lower TMA exposures on hydroxyl-terminated and ethyl-terminated ZnO films. More mass loss was observed on ethyl-terminated ZnO films compared with hydroxyl-terminated films, because TMA does not have the possibility of reacting with hydroxyl groups on ethyl-terminated ZnO films. The mass losses also increased progressively with temperatures ranging from 100 to 225 °C on both hydroxyl-terminated and ethyl-terminated ZnO films. The perspective concludes with a discussion of the generality of conversion reactions in atomic layer processing.

I. INTRODUCTION

Sequential, self-limiting surface reactions are the basis of atomic layer deposition (ALD) and thermal atomic layer etching (ALE).[1,2] Gas phase precursors are incident on surfaces during atomic layer processing. For ALD, most of these reactions are believed to be restricted to the surface species.[3] For thermal ALE, these reactions are also thought to be confined to the surface species or the near surface region.[2] However, missing from these assumptions is the possibility that gaseous precursors can also convert surfaces to new materials.

The most common surface reaction during the ALD of metal oxides is the reaction of a metal precursor with surface hydroxyl groups on the initial metal oxide.[1,3] This reaction is given as

$$MOH^* + NL_x(g) \rightarrow MO - NL_{x-1}^* + LH(g). \quad (1)$$

In this reaction, M is the metal of the initial metal oxide, N is the metal of the incoming metal precursor, and L is a ligand on the metal precursor. The asterisks denote the surface species. This

reaction is especially important during ALD nucleation. This simple picture for the ALD surface reaction ignores the possibility that the metal precursor could convert the initial metal oxide surface.

Depending on the reaction thermochemistry, the metal precursor can also undergo a conversion reaction with the initial metal oxide.[4–6] This conversion reaction involves the exchange between the two metals and can be very generally written as

$$MO_w + NL_x(g) \rightarrow NO_y + ML_z(g). \quad (2)$$

This conversion reaction may be possible if the new oxide being formed, NO_y, is more stable than the original metal oxide, MO_w. In addition, the metal of the original oxide needs to form a volatile species with the ligands of the incoming metal precursor. The metal of the incoming metal precursor can then exchange with the metal of the initial metal oxide and form a more stable new metal oxide. Thermochemical calculations can be utilized to measure the potential for various conversion reactions. Metal oxide conversion involves the exchange of metal cations. Other types of conversion reactions may involve the exchange of anions.

This perspective describes conversion reactions in atomic layer processing. Previous examples of conversion reactions will first be reviewed from many areas, including ALD and ALE. The conversion of ZnO to Al_2O_3 by trimethylaluminum (TMA) will then be described as a model conversion system. The ZnO conversion to Al_2O_3 will be documented by a variety of experiments, including FTIR spectroscopy, mass spectrometry, x-ray reflectivity (XRR), gravimetric measurements, x-ray photoelectron spectroscopy (XPS), and quartz crystal microbalance (QCM) studies. The perspective will close with a discussion of the pervasiveness and usefulness of conversion reactions during atomic layer processing.

II. PREVIOUS EXAMPLES OF CONVERSION REACTIONS

A. Atomic layer deposition of layered structures and alloys

Conversion reactions have been documented previously during the ALD of alloys and nanolaminates.[7] One of the early observations of conversion was during the growth of ZnO/Al_2O_3 nanolaminates using ZnO ALD and Al_2O_3 ALD.[8] ZnO ALD was performed with $Zn(CH_2CH_3)_2$ and H_2O as the reactants. Al_2O_3 ALD was conducted using TMA and H_2O as the reactants. In this study, *in situ* QCM measurements showed a significant mass loss of ~62 ng/cm^2 during the nucleation of Al_2O_3 ALD on ZnO when TMA was exposed to a hydroxyl-terminated ZnO surface.[8] These *in situ* QCM measurements are displayed in Fig. 1.[8] This significant mass loss can be explained by the conversion of ZnO to Al_2O_3 through the exchange of metal cations according to

$$3ZnO + 2Al(CH_3)_3(g) \rightarrow Al_2O_3 + 3Zn(CH_3)_2(g). \quad (3)$$

In addition to the large mass loss when exposing TMA to the hydroxylated ZnO surface, there was a lower zinc content in the ZnO/Al_2O_3 nanolaminate films than expected from rule-of-mixture predictions. This lower zinc concentration was explained as resulting from the etching of ZnO by TMA.[8] Subsequent mass spectrometric studies also identified $Zn(CH_3)_2$ as a reaction product

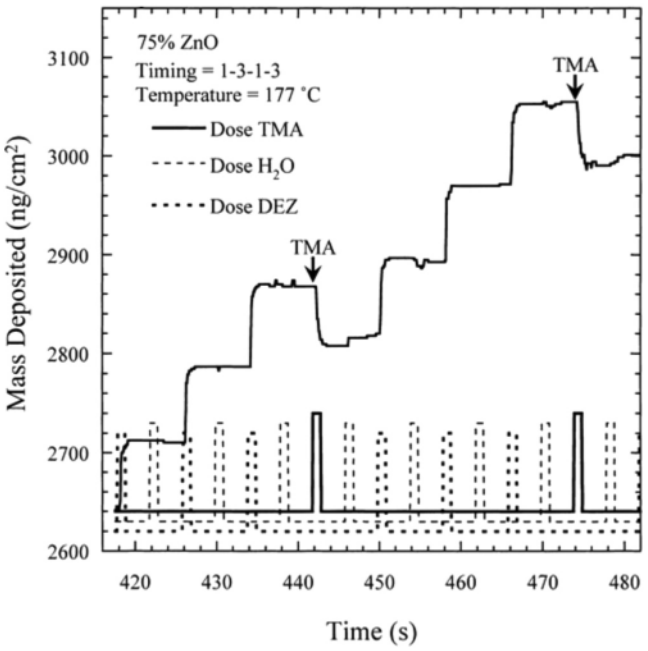

FIG. 1. QCM measurements of mass changes during the deposition of a ZnO/Al_2O_3 alloy film using ZnO ALD and Al_2O_3 ALD (Ref. 8). TMA exposure on the hydroxylated ZnO surface shows a large mass decrease of ~62 ng/cm^2. Reprinted with permission from Elam and George, Chem. Mater. **15**, 1020 (2003). Copyright 2003, American Chemical Society.

during TMA exposures on ZnO surfaces.[9] Etching of ZnO by CH_4 plasma also supports the removal of Zn by the formation of $Zn(CH_3)_2$.[10]

Another example of conversion by the exchange of metal cations occurs during the ALD growth of $ZnIn_xS_y$ alloys using alternating ZnS ALD and In_2S_3 ALD cycles.[11,12] During the alloy growth, $Zn(CH_2CH_3)_2$ is able to convert In_2S_3 to ZnS according to

$$In_2S_3 + 3Zn(CH_2CH_3)_2(g) \rightarrow 3ZnS + 2In(CH_2CH_3)_3(g). \quad (4)$$

This conversion reaction leads to $ZnIn_xS_y$ alloy compositions that deviate dramatically from the expected predictions based on the rule of mixtures.[11,12]

The exchange of metal cations also affects the ALD growth of Cu_2S/ZnO layered structures using Cu_2S ALD and ZnO ALD.[13] When $Zn(CH_2CH_3)_2$ is incident on a Cu_2S substrate, the surface of the Cu_2S substrate can be converted to ZnS according to

$$Cu_2S + Zn(CH_2CH_3)_2(g) \rightarrow ZnS + 2Cu + C_4H_{10}(g). \quad (5)$$

Likewise, when the Cu precursor, $Cu_2(DBA)_2$ [bis(N,N'-disec-butylacetamidinato)dicopper(I)] is incident on the ZnS substrate, the surface of the ZnS substrate can be converted to

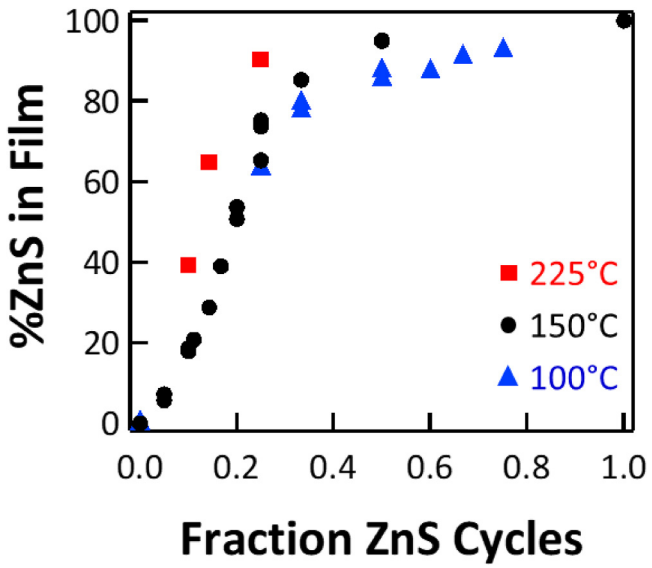

FIG. 2. Percent ZnS in Zn(O,S) films grown using alternating cycles of ZnS ALD and ZnO ALD at 100, 150, and 225 °C (Ref. 14). Zn(O,S) films have much more sulfur than expected compared with the fraction of ZnS cycles. Reprinted with permission from Lancaster *et al.*, J. Phys. Chem. C **121**, 18643 (2017). Copyright 2017, American Chemical Society.

Cu_2S according to[13]

$$ZnS + Cu_2(DBA)_2(g) \rightarrow Cu_2S + Zn(DBA)_2(g). \quad (6)$$

Other conversion reactions involving the exchange of anions have also been observed during the ALD of Zn(O,S) alloys using ZnO ALD and ZnS ALD.[14–16] ZnO ALD was performed with $Zn(CH_2CH_3)_2$ and H_2O as the reactants. ZnS ALD was conducted using $Zn(CH_2CH_3)_2$ and H_2S as the reactants. For the Zn(O,S) alloys, the conversion occurs between the O and S anions. The Zn(O,S) alloys deposited using ZnO ALD and ZnS ALD have a much higher sulfur content than expected based on the fraction of ZnS ALD cycles used to deposit the Zn(O,S) alloy.[14] The %ZnS in the film as a function of the fraction of ZnS cycles used to grow the Zn(O,S) alloy growth is shown in Fig. 2.[14]

The high sulfur content at a low fraction of ZnS cycles is attributed to the reaction of the H_2S (hydrogen sulfide) with the ZnO substrate.[14,16] Typically, switching between ZnO ALD and ZnS ALD when growing the Zn(O,S) alloy will result in the reaction of H_2S with the $Zn–CH_2CH_3$* species from the previous ZnO ALD cycle. However, H_2S can also react with the underlying ZnO surface according to

$$ZnO + H_2S(g) \rightarrow ZnS + H_2O(g). \quad (7)$$

This conversion reaction increases the S concentration in the Zn(O,S) alloy.[14] This exchange between O and S leads to difficulty when trying to control the composition of the Zn(O,S) alloy. Figure 2 also shows that the O/S exchange reaction is more efficient at higher temperatures.[14] For temperatures of 100, 150, and 225 °C, at a ratio of 3:1 ZnO:ZnS ALD cycles, the %ZnS in the Zn(O,S) alloy was 65%, 75%, and 90%, respectively.[14]

B. Self-cleaning during atomic layer deposition

Conversion has also been observed during the nucleation of ALD films on underlying substrates. This conversion has been used to remove unwanted oxides from the initial substrates. The conversion occurs during the initial metal precursor reaction during ALD, because the new metal oxide is more stable than the original metal oxide. There are many investigations of ALD "self-cleaning" on semiconductor surfaces, including GaAs, InGaAs, and other compound semiconductor substrates.[17] Most of these studies have employed TMA for Al_2O_3 ALD or TEMA–Hf or TDMA–Hf for HfO_2 ALD. TEMA–Hf is tetrakis(ethylmethylamino)hafnium and TDMA–Hf is tetrakis(dimethylamino)hafnium.

Many investigations have explored the removal of AsO_x and GaO_x oxides from GaAs substrates. For example, the reaction of TMA or TEMA-Hf with AsO_x and GaO_x on GaAs can remove these oxides and deposit Al_2O_3 or HfO_2, respectively.[18] An illustration of this oxide removal is given by the XPS results for As 2p and Ga 2p in Fig. 3.[18] There is a dramatic reduction in both the arsenic and gallium oxide peaks after the Al_2O_3 ALD or HfO_2 ALD. Other XPS studies have also observed the removal of oxides on GaAs or $In_xGa_{(1-x)}As$ using TMA, TEMA–Hf, or TDMA–Hf.[17,19–22] The Al 2p peak in the XPS spectrum also increased as the native oxides were removed from the substrate.[20,21,23] The disappearance of the native oxide, together with the production of the Al 2p XPS signal from Al_2O_3, is consistent with a conversion reaction.

In addition to the XPS studies, high resolution transmission electron microscopy (HRTEM) investigations have also revealed that the native oxides are removed by HfO_2 ALD on InGaAs using TEMA–Hf and H_2O as the precursors.[19] Figure 4(a) shows the HRTEM image of a native oxide with a thickness of 2.4 nm on the InGaAs substrate.[19] Figure 4(b) then displays the HRTEM image after depositing a HfO_2 ALD film with a thickness of 7.4 nm on the InGaAs substrate.[19] There is a sharp interface between HfO_2 and InGaAs with no evidence for the original native oxide. The absence of the native oxide in Fig. 4(b) is attributed to "ligand-exchange" reactions between TEMA–Hf and the native oxides on InGaAs that convert the native oxides to HfO_2.[19] These "clean up" reactions that lead to surface conversion have also been modeled using density functional theory calculations.[4,5]

C. Atomic layer etching

Surface exchange reactions and conversion are also important during some thermal atomic layer etching (ALE) processes. Similar to ALD, thermal ALE is based on sequential, self-limiting surface reactions.[2] However, an atomic layer of material is removed during each thermal ALE cycle instead of an atomic layer of material being added during each ALD cycle. Thermal ALE can proceed by surface modification and then by the volatile release of the modified surface layer.[2] One well established pathway for thermal ALE is fluorination to modify the surface and then ligand-exchange to produce volatile etch products.[2,24,25]

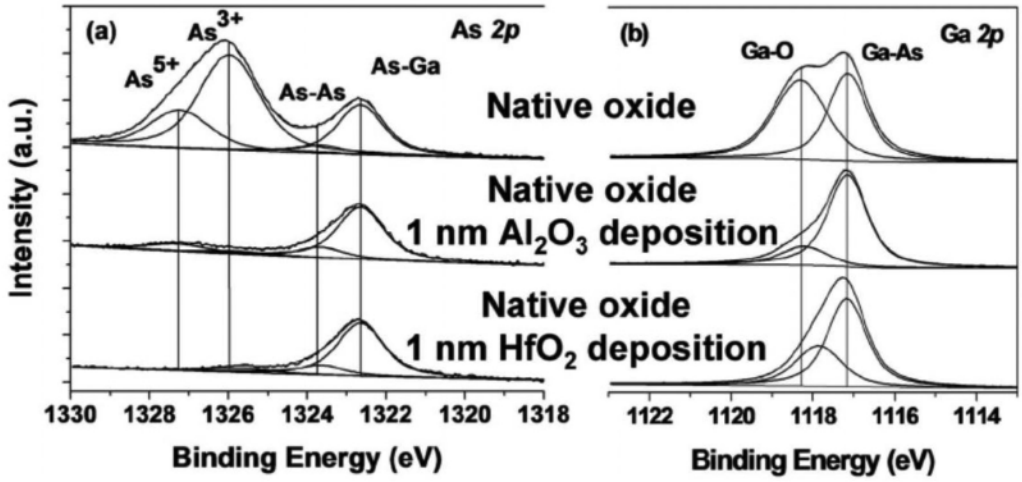

FIG. 3. XPS spectra of (a) As 2p 3/2 and (b) Ga 2p 3/2 showing oxidation state differences for a native oxide on a GaAs surface and after Al_2O_3 ALD and HfO_2 ALD (Ref. 18). Al_2O_3 ALD and HfO_2 ALD removes the higher oxidation states of As and Ga. Reprinted with permission from Hinkle *et al.*, Appl. Phys. Lett. **92**, 071901 (2008). Copyright 2008, American Institute of Physics LLC.

Because thermal ALE utilizes metal precursors for the ligand-exchange reaction, there is a possibility that the metal precursor could both react with the surface fluoride layer by ligand-exchange and then proceed to undergo a conversion reaction with the underlying substrate. One example of a conversion reaction during thermal ALE is ZnO ALE using HF and TMA as the reactants.[26] A mass loss was observed by quartz crystal microbalance (QCM) studies when the ZnF_2 surface was exposed to TMA following HF exposure on ZnO.[26] This mass loss was much higher than expected for only the ligand-exchange reaction. This additional mass loss was attributed to the reaction of TMA with the underlying ZnO substrate that converted the surface of the ZnO layer to Al_2O_3.[26]

Conversion can be especially important when trying to etch materials that cannot be etched using the traditional fluorination and ligand-exchange etching method. For example, some materials do not have viable pathways for thermal ALE because they do not form stable and volatile etch products.[27] The surface of these materials may be converted to a different surface layer that leads to stable and volatile etch products.

Thermal SiO_2 ALE is an example of surface conversion that enables the etching of SiO_2.[28] During thermal SiO_2 ALE, TMA is able to convert the surface of SiO_2 to an Al_2O_3 surface layer.[28] The Al_2O_3 layer can then be fluorinated to AlF_3 and subsequently removed by a ligand-exchange reaction using TMA. Note that TMA provides for both the ligand-exchange and conversion reactions. An illustration of the surface chemistry for thermal SiO_2 ALE is shown in Fig. 5.[28] Thermal Si and Si_3N_4 ALE are based on thermal SiO_2 ALE and utilize oxidation to SiO_2 and then the conversion of SiO_2 to Al_2O_3.[29,30]

Another example of a conversion reaction for thermal ALE is WO_3 ALE using BCl_3 and HF as the reactants.[31] Conversion is important because the fluorination of WO_3 by HF is thermochemically unfavorable. Fortunately, BCl_3 can convert the WO_3 surface to a B_2O_3 surface layer, because B_2O_3 is a much more stable oxide than WO_3. Subsequently, HF can spontaneously remove the B_2O_3 surface layer.[31] The etching of WO_3 by BCl_3 and HF can also be extended to W ALE after oxidizing W to WO_3 using an O_2/O_3 mixture.[31]

III. EXPERIMENTAL FOR ZnO CONVERSION TO Al_2O_3

A. FTIR spectroscopy

In situ FTIR experiments were conducted to study ZnO conversion to Al_2O_3 by TMA and the species on the initial ZnO surface and the resulting Al_2O_3 surface. These experiments were performed in a vacuum reactor reported earlier.[32] To obtain adequate surface sensitivity, FTIR studies were performed in transmission mode using silicon nanoparticles that were 30–50 nm in diameter.

The silicon particles were pressed into a tungsten grid that was $2 \times 3\ cm^2$, 50 μm thick with 100 grid lines per inch. The grid was resistively heated by a DC power supply (6268B, 20 V/20 A, Hewlett-Packard) to a temperature of 150 °C. The temperature was measured with a type K thermocouple that was attached to the tungsten grid using a nonconductive high temperature epoxy (Ceramabond 571, Aremco).

ZnO ALD films were deposited on the silicon particles. ZnO ALD was performed at 150 °C using diethylzinc (Sigma Aldrich, 99.5% pure) and reagent grade water (Sigma Aldrich).[33] FTIR spectroscopy studied the reaction of TMA (97%, Sigma-Aldrich) on the ZnO ALD films that were on the silicon particles at 150 °C. The TMA exposures were composed of multiple TMA doses. Each TMA dose was conducted for 1 s at 100 mTorr.

B. Quadrupole mass spectrometry

The volatile products during TMA exposures on ZnO were studied using quadrupole mass spectrometry. The experiments

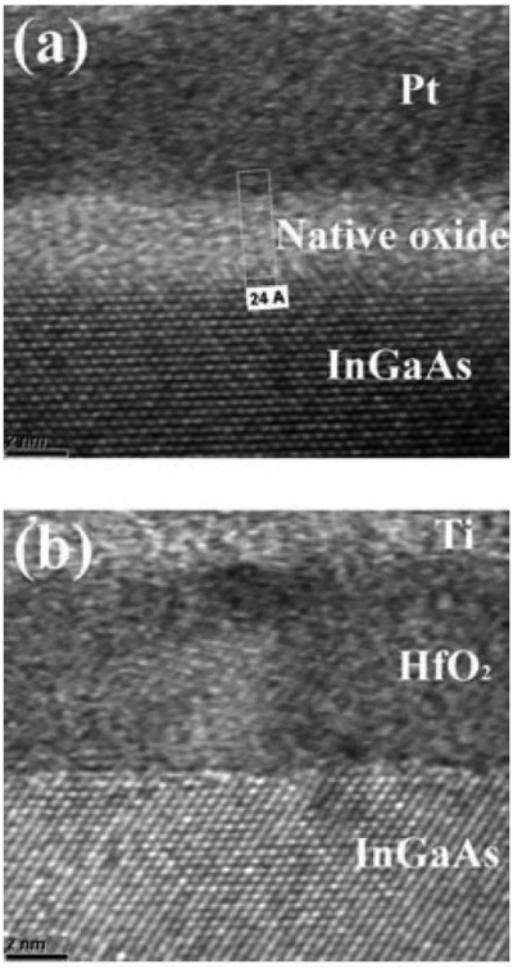

FIG. 4. Cross-sectional HRTEM images of (a) InGaAs substrate with a native oxide thickness of 2.4 nm and (b) InGaAs substrate with HfO_2 coating of 7.4 nm after HfO_2 ALD (Ref. 19). HfO_2 ALD removes the native oxide on InGaAs. Reprinted with permission from Chang *et al.*, Appl. Phys. Lett. **89**, 242911 (2006). Copyright 2006, American Institute of Physics LLC.

were conducted in a vacuum reactor that has been described previously.[34] The volatile products resulting from TMA exposure on ZnO were studied using 500 mg of Al_2O_3 powder (40–50 nm APS, Nanophase) coated with ZnO ALD. ZnO ALD was performed at 150 °C using diethylzinc (Sigma Aldrich, 99.5% pure) and reagent grade water (Sigma Aldrich).

The Al_2O_3 powder had a high surface area of 32–40 m^2/g to produce a large quantity of volatile reaction products. In addition, the high surface area of the Al_2O_3 powder greatly exceeded the surface area of the chamber walls. The conversion reaction was studied on both hydroxyl-terminated and ethyl-terminated ZnO powder using TMA (97%, Sigma-Aldrich). Initial TMA exposures into the clean vacuum reactor without the ZnO-coated Al_2O_3 powder did not reveal any impurities in the TMA using quadrupole mass spectrometry (QMS).

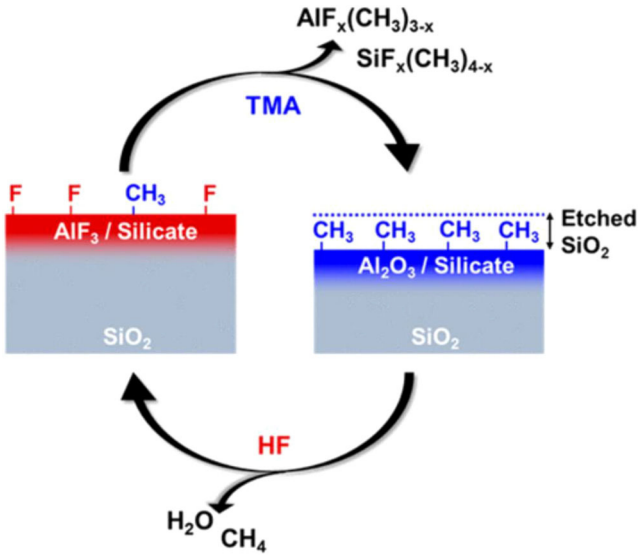

FIG. 5. Schematic of the proposed reaction mechanism for SiO_2 ALE by "conversion-etch" using the sequential exposures of HF and TMA (Ref. 28). TMA converts SiO_2 to an Al_2O_3/silicate surface layer. Reprinted with permission from DuMont *et al.*, ACS Appl. Mater. Interfaces **9**, 10296 (2017). Copyright 2017, American Chemical Society.

In situ QMS analysis of the fluorination and ligand-exchange reactions was performed at 150 °C under static dosing conditions. For the exchange reaction, 4 Torr of TMA was held statically in the reaction chamber for 60 s before purging. Every precursor exposure was followed by a purging sequence of 120 s of static N_2 purge, 240 s of viscous N_2 purge, and final 120 s of static N_2 purge to prevent cross-contamination between reactant precursors.

QMS sampling was performed during the reactant exposures.[34] At the onset of the reactant exposure, a pneumatic valve was opened between the reaction chamber and the QMS ionization region. QMS scans were repeated continuously for 60 s. Each QMS scan from $m/z = 0$ to 300 required 6 s. Ten scans were conducted during the 60 s exposure. The QMS spectra were largely unchanged after the second scan. The first scan could be affected by adsorbed gases on the powder sample and the chamber walls that are present after atmospheric exposures when loading the samples.

C. Rotary particle reactor

Experiments at high TMA exposure were performed on ZnO particles in a hot-walled static rotary particle reactor. This rotary particle reactor has been described previously.[35] The rotary particle reactor is equipped with a magnetic feedthrough (UHV Transfer Systems) that extends into the reactor chamber. A motor powered by a DC regulated power supply (BK Precision 1670A) rotates an outer housing of SmCo magnets. These magnets rotate a rotary armature made of magnetic steel inside the vacuum system. As this armature rotates, the shaft extending into the reactor chamber connects to a porous stainless steel canister and rotates this canister.

The rotating canister houses the ZnO nanoparticles. The rotation provides agitation of the ZnO nanoparticles and allows the gas exposures to access the entire surface area of the ZnO nanoparticles. The reactor was pumped down and purged using a dual-stage rotary vane mechanical pump. Pressure was measured using a capacitance manometer (Baratron). Nitrogen (UHP Airgas) was used as a purging gas.

The ZnO nanoparticles were synthesized using $ZnCl_2$ (Sigma Aldrich) and NaOH in an ethylene glycol medium (Sigma Aldrich) at 150 °C and vacuum dried overnight.[36] The nanoparticles were approximately 10 nm in diameter. ZnO films were also deposited on witness wafers. These ZnO ALD films were grown using diethylzinc (DEZ) (Sigma Aldrich, 99.5% pure) and deionized water using a Beneq TFS-200 ALD system. The DEZ and H_2O dose times were 3 s and 1 s, respectively.

The mass, thickness, and composition change were investigated after the exposure of the ZnO nanoparticles to TMA (Sigma Aldrich, 97% pure). TMA exposures ranged from 5 Torr s to 1200 Torr s. Each exposure consisted of multidoses of 1 Torr of TMA for 60 s. For example, the 1200 Torr s exposure consisted of 20 consecutive 60 s doses of TMA at 1 Torr. Each TMA exposure was followed by a 60 s static N_2 purge, a 90 s N_2 purge at 9 Torr, and another 90 s static N_2 purge to ensure all excess TMA and reaction products were removed from the chamber. The reactor temperature was varied between 150 and 220 °C.

Particle and film elemental compositions were obtained using a PHI 5600 x-ray photoelectron spectrometer. The ZnO ALD films were also characterized using witness wafers in the rotary particle reactor. *Ex situ* thickness measurements of the films on these witness wafers were performed with an x-ray reflectometer (Bede D1, Jordan Valley Semiconductors).

D. Quartz crystal microbalance measurements

The mass changes during ZnO ALD, Al_2O_3 ALD, and growth of ZnO/Al_2O_3 nanolaminates were monitored using quartz crystal microbalance (QCM) measurements.[8] These experiments were conducted in a hot-walled viscous flow reactor.[37] A nitrogen flow (UHP Airgas) of 150 SCCM entered the front of the reactor through two gas lines. The reactor pressure was maintained at ~1 Torr using this nitrogen flow coupled with pumping by a dual-stage rotary vane mechanical pump. Pressure was monitored using a capacitance manometer. The reactor temperature was varied between 100 and 225 °C.

ZnO films were grown using diethylzinc (Sigma Aldrich, 99.5% pure) and de-ionized water as precursors.[8] Al_2O_3 films were grown using TMA (Sigma Aldrich, 97% pure) and de-ionized water.[8] The precursor dose time was 0.3 s for growing all the films. The exposure of each precursor was varied by changing the pressure of the dose. Each exposure was maintained within the following limits: 0.4–0.5 Torr s for H_2O, 0.5–0.6 Torr s for DEZ, and 0.8–0.9 Torr s for TMA. Purge times following each precursor exposure were constant at 30 s. This purge time was sufficient to prevent chemical vapor deposition (CVD) at the lowest temperature of 100 °C.

Nanolaminates were grown using *x* cycles of ZnO ALD followed by *x* cycles of Al_2O_3 ALD.[38] This notation is designated by x ZnO cycles: x Al_2O_3 cycles. For example, a value of x = 5 is consistent with a sequence of 5 cycles of ZnO ALD followed by 5 cycles of Al_2O_3 ALD. The conversion reaction was investigated by observing mass changes on the first TMA exposure during Al_2O_3 ALD on the underlying ZnO ALD film. Experiments showed that the mass changes during the conversion of ZnO to Al_2O_3 by TMA varied with the number of previous ZnO ALD cycles. However, the mass changes were nearly insensitive to the number of Al_2O_3 ALD cycles prior to ZnO ALD.

QCM measurements were performed using a 6 MHz AT-cut crystal sealed within a BSH-150 (Inficon) bakeable sensor head. Growth rates during pure Al_2O_3 ALD and ZnO ALD were measured at 33 and 110 ng/cm^2, respectively. These mass changes per cycle during ALD agree well with previous literature values.[8,37]

IV. RESULTS FOR ZnO CONVERSION TO Al_2O_3 BY TRIMETHYLALUMINUM

Trimethylaluminum (TMA) is one of the most well-known metal precursors for ALD and ALE.[3,39] TMA is used in many atomic layer processes because of its exceptional reactivity and high vapor pressure. TMA is the source of aluminum for the flagship process of Al_2O_3 ALD.[1,3] TMA is also a common metal precursor used for ligand-exchange during many thermal ALE processes.[26,28,39] TMA has also been employed in surface cleaning to remove native oxides.[18,20,21,23]

During Al_2O_3 ALD on ZnO, TMA can react with surface hydroxyl groups according to

$$ZnOH^* + Al(CH_3)_3(g) \rightarrow ZnO - Al(CH_3)_2^* + CH_4(g). \quad (8)$$

In addition, TMA also has the opportunity to convert ZnO to Al_2O_3 based on the reaction given in Eq. (3). This reaction is also illustrated in Fig. 6. This conversion reaction is likely to occur because the thermochemistry for the conversion to Al_2O_3 is favorable. Equation (3) has a standard free energy change of $\Delta G° = -165$ kcal/mol as determined by thermochemical calculations.[40]

ZnO and Al_2O_3 are two of the most well-studied and understood oxide ALD systems.[1,3,41,42] Al-doped ZnO (AZO) is an important transparent conducting oxide.[43] Many studies have investigated the electrical properties of Al-doped ZnO ALD films.[44–48] Other investigations have focused on the growth and characterization of ZnO/Al_2O_3 nanolaminates deposited using various numbers of ZnO ALD and Al_2O_3 ALD cycles.[38,49,50]

This investigation will use a number of analytical techniques to characterize the conversion of ZnO to Al_2O_3 using TMA. This case study will concentrate on the conversion of ZnO to Al_2O_3 as measured by surface reactions, bulk reactions, and gas phase reaction products. In addition, the investigations will examine two different ZnO surfaces: hydroxyl-terminated and ethyl-terminated surfaces. The surface species may have an effect on the extent and the mechanism of the conversion reaction. The reaction of TMA with ZnO surfaces may involve competition between surface and bulk reactions. The idea of self-limiting surface reactions during ALD may need to be revisited if there is an opportunity for surface conversion.

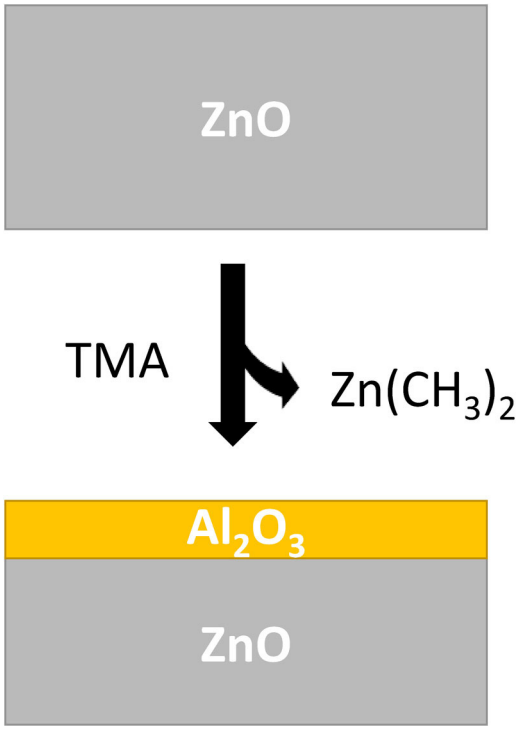

FIG. 6. Schematic of the proposed conversion reaction of ZnO to Al_2O_3 using TMA. Exposure to TMA results in the conversion of ZnO to Al_2O_3 with $Zn(CH_3)_2$ as the gaseous by-product.

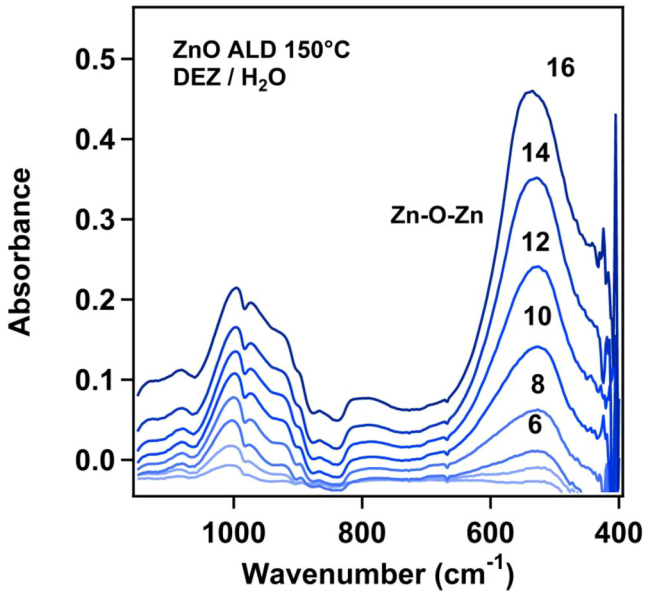

FIG. 7. FTIR spectra of ZnO ALD growth using sequential DEZ and H_2O exposures at 150 °C. Each FTIR spectrum was obtained after two ZnO ALD cycles.

A. FTIR spectroscopy

In situ FTIR spectroscopy was used to understand the surface chemistry during TMA exposure to the ZnO surface. During these experiments, ZnO surfaces terminated with different species were exposed to TMA. Initially, ZnO films were grown using ZnO ALD with DEZ and H_2O as the reactants.[33] Figure 7 shows the growth of ZnO ALD films at 150 °C versus the number of ZnO ALD cycles. The two sequential, self-limiting surface reactions during ZnO ALD are[33]

$$\text{(A)}\quad \mathrm{ZnOH^*}+\mathrm{Zn(CH_2CH_3)_2}(g)\rightarrow \mathrm{ZnO-ZnCH_2CH_3^*}+\mathrm{C_2H_6}(g), \tag{9}$$

$$\text{(B)}\quad \mathrm{ZnCH_2CH_3^*}+\mathrm{H_2O}(g)\rightarrow \mathrm{Zn-OH^*}+\mathrm{C_2H_6}(g). \tag{10}$$

Figure 7 shows that there are two peaks related to Zn–O vibrational modes in the infrared region below 1200 cm^{-1}. The absorbance peak centered at 530 cm^{-1} is characteristic of the bulk Zn–O vibrational mode.[51–53] The peaks between 900 and 1050 cm^{-1} are attributed to ZnO silicate vibrational modes at the interface between the ZnO ALD film and the SiO_2 layer on the Si particles. This absorbance feature grows during the first few ZnO ALD cycles and is then relatively constant for thicker ZnO ALD films. There is an increase in the background absorbance versus the number of ZnO ALD cycles, which is apparent at ≥1100 cm^{-1}. This rising background absorbance is caused by free carrier absorption in ZnO and has been observed previously.[33]

FTIR studies were then performed on the ZnO ALD films terminated by either $ZnOH^*$ or $ZnCH_2CH_3^*$ species. These two different surface terminations were prepared by ending the ZnO ALD reaction sequence with either an H_2O or $Zn(CH_2CH_3)_2$ exposure. Figure 8 shows difference spectra after a hydroxyl-terminated ZnO surface was exposed to the first TMA dose at 150 °C. The reference spectrum was the previous spectrum of the hydroxylated ZnO surface. The surface reaction of TMA with a hydroxyl-terminated ZnO surface is given by Eq. (8). Consistent with the change expected from Eq. (8), Fig. 8(a) displays an absorbance loss for the O–H stretching vibration at 3670 cm^{-1} and an absorbance gain for the C–H stretching vibration at 2900 cm^{-1}. These changes are in agreement with the loss of surface $ZnOH^*$ species and a gain of surface $AlCH_3^*$ species.

Figure 8(b) shows the FTIR difference spectrum at lower frequencies between 400 and 1100 cm^{-1} for TMA exposure on the hydroxyl-terminated ZnO surface. As expected from Eq. (3), conversion leads to an absorbance loss of the Zn–O vibration and absorbance gain of Al–O vibrational features. The two distinct Al–O vibrational modes are observed that are assigned to Al–O–Zn and Al–O–Al vibrations located at 715 and 810 cm^{-1}, respectively.[54–56] The TMA dose also leads to the appearance of an $Al–CH_3$ deformation peak at 1215 cm^{-1} that is consistent with $Al–CH_3^*$ species on the surface.[54,57]

The hydroxyl-terminated ZnO surface was then exposed to additional TMA doses. Figure 9 displays difference spectra after the

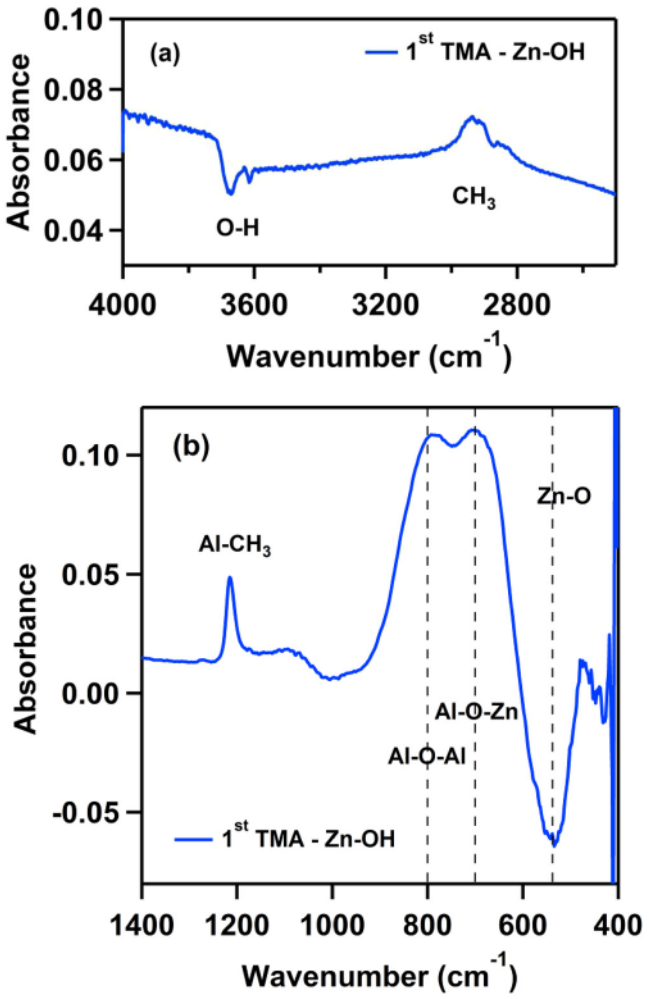

FIG. 8. FTIR difference spectrum showing an absorbance of (a) O-H and C-H stretching vibrations and (b) Al–O and Zn–O vibrational modes after the hydroxyl-terminated ZnO surface was exposed to the first TMA dose at 150 °C. The reference spectrum was obtained from the hydroxyl-terminated ZnO surface.

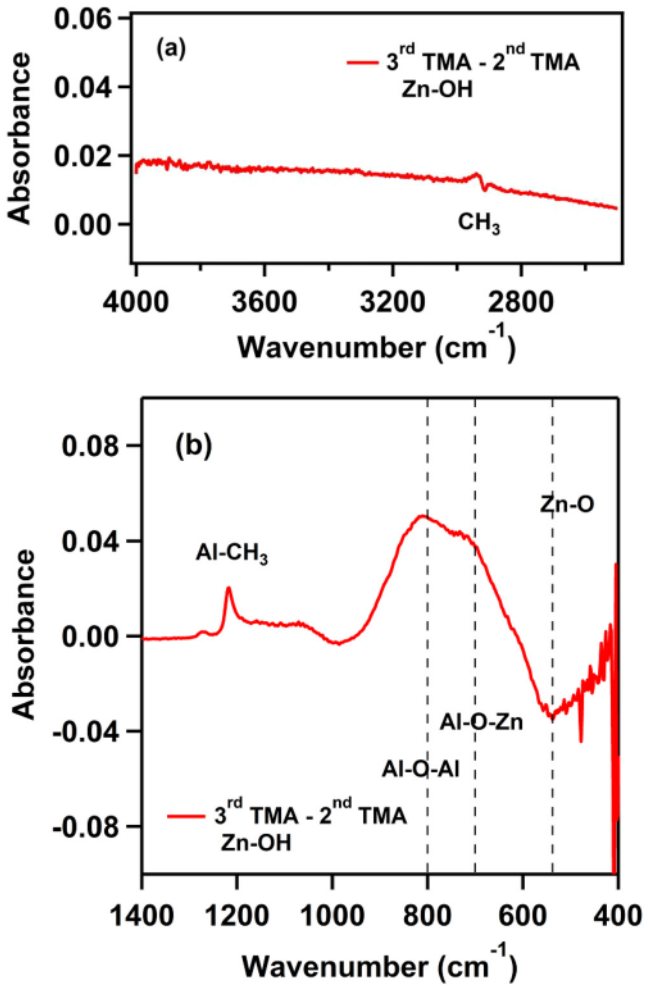

FIG. 9. FTIR difference spectrum showing the absorbance of (a) O–H and C–H stretching vibrations and (b) Al–O and Zn–O vibrational modes after the hydroxyl-terminated ZnO surface was exposed to the third TMA dose at 150 °C. The reference spectrum was obtained after the second TMA dose.

third TMA dose referenced to the spectra after the second TMA dose. Figure 9(a) shows that the third TMA dose leads to no change in the O–H or C–H vibrational stretching region. The TMA surface reactions have reached completion. There is no additional loss of ZnOH* species and gain of $AlCH_3$* species, as observed in Fig. 8(a). In contrast, Fig. 9(b) reveals that the conversion from ZnO to Al_2O_3 continues with additional TMA doses. Figure 9(b) shows the absorbance loss of the Zn–O mode and the absorbance gain of Al–O–Zn and Al–O–Al vibrations. The ZnO conversion to Al_2O_3 continues after the initial surface reactions reach saturation.

Figure 10 displays the progressive absorbance loss of the Zn–O vibrational mode and the absorbance gain of Al–O–Zn and Al–O–Al vibrations with the number of TMA doses for the hydroxyl-terminated ZnO surface at 150 °C. The largest conversion of ZnO to Al_2O_3 occurs during the first several TMA doses. The amount of additional conversion progressively decreases with each TMA dose. However, there is still some additional conversion even after 10 TMA doses. This behavior is expected if the converted Al_2O_3 layer on the ZnO surface acts as a diffusion barrier for additional conversion. The kinetics of this conversion may be similar to the Deal–Grove model for silicon oxidation where the SiO_2 layer acts as a diffusion barrier for additional oxidation.[58]

Figure 11 displays the difference spectra after the ethyl-terminated ZnO surface was exposed to the first TMA dose. Figure 11(a) displays only a small absorbance loss in the C–H stretching vibration region at ~2900 cm^{-1}. This small absorbance

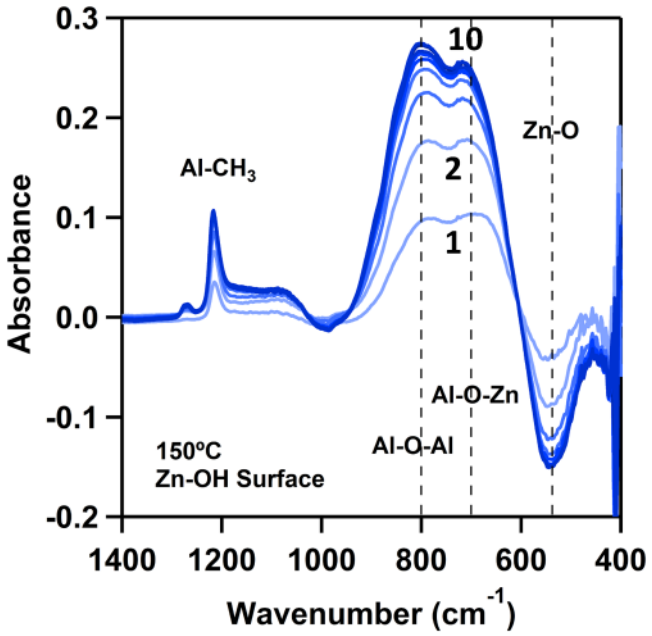

FIG. 10. FTIR difference spectra showing the absorbance of Al-O and Zn-O vibrational modes during consecutive TMA doses on a hydroxyl-terminated ZnO surface at 150 °C.

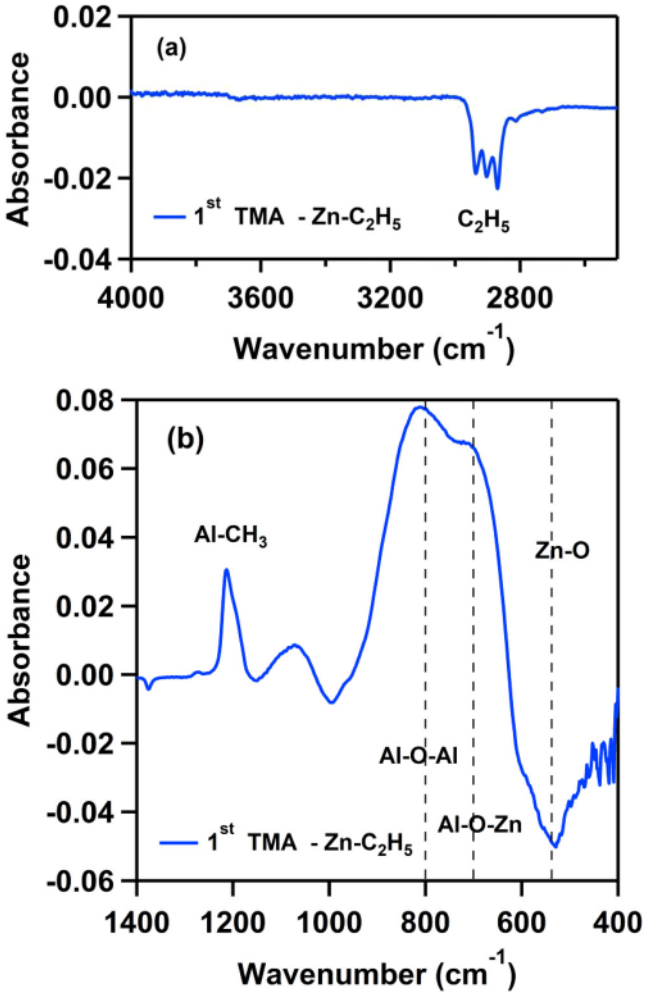

FIG. 11. FTIR difference spectrum showing the absorbance of (a) O–H and C–H stretching vibrations and (b) Al–O and Zn–O vibrational modes after the ethyl-terminated ZnO surface was exposed to the first TMA dose at 150 °C. The reference spectrum was obtained from the ethyl-terminated ZnO surface.

loss is consistent with some exchange between $-CH_3$ on TMA and $-CH_2CH_3$ on the ethyl-terminated surface. In contrast, there are large absorbance changes observed at lower frequencies in Fig. 11(b). Similar to Fig. 8(b), there is an absorbance loss of the Zn–O vibrational mode at 535 cm^{-1} and an absorbance gain of Al–O–Zn and Al–O–Al vibrations located at 715 and 810 cm^{-1}. The conversion of ZnO to Al_2O_3 occurs for both hydroxyl-terminated and ethyl-terminated ZnO surfaces.

The ethyl-terminated ZnO surface was then exposed to additional TMA doses. Figure 12 displays difference spectra after the third TMA dose is referenced to the spectra after the second TMA dose. Figure 12(a) shows that the third TMA dose leads to no change in the C–H vibrational stretching region. There is no additional exchange between TMA and the ethyl-terminated ZnO surface. In contrast, Fig. 12(b) reveals that the conversion from ZnO to Al_2O_3 continues with additional TMA doses. Figure 12(b) shows the absorbance loss of the Zn–O vibrational mode and the absorbance gain of Al–O–Zn and Al–O–Al vibrations. Similar to Fig. 9, the ZnO conversion to Al_2O_3 can proceed after the initial surface reactions reach saturation.

Figure 13 displays the progressive absorbance loss of the Zn–O vibrational mode and the absorbance gain of Al–O–Zn and Al–O–Al vibrations with the number of TMA doses for the ethyl-terminated ZnO surface at 150 °C. Similar to Fig. 10, the largest conversion of ZnO to Al_2O_3 occurs during the first several TMA doses. The amount of additional conversion progressively decreases with each TMA dose. However, there is still some additional conversion even after 10 TMA doses. As mentioned above to explain the behavior in Fig. 10, this behavior is expected if the converted Al_2O_3 layer on the ZnO surface acts as a diffusion barrier for additional conversion.

B. Mass spectrometry

To understand the mechanism of conversion, mass spectrometry studies were employed to identify the gaseous species produced during TMA exposures on the ZnO surface. For these experiments, ZnO ALD films were deposited on high surface area Al_2O_3 particles. By ending the ZnO ALD reaction sequence with either a H_2O exposure or DEZ exposure, the ZnO ALD films were left with either hydroxyl termination or ethyl termination. According to Eq. (8), TMA is expected to react on a hydroxyl-terminated

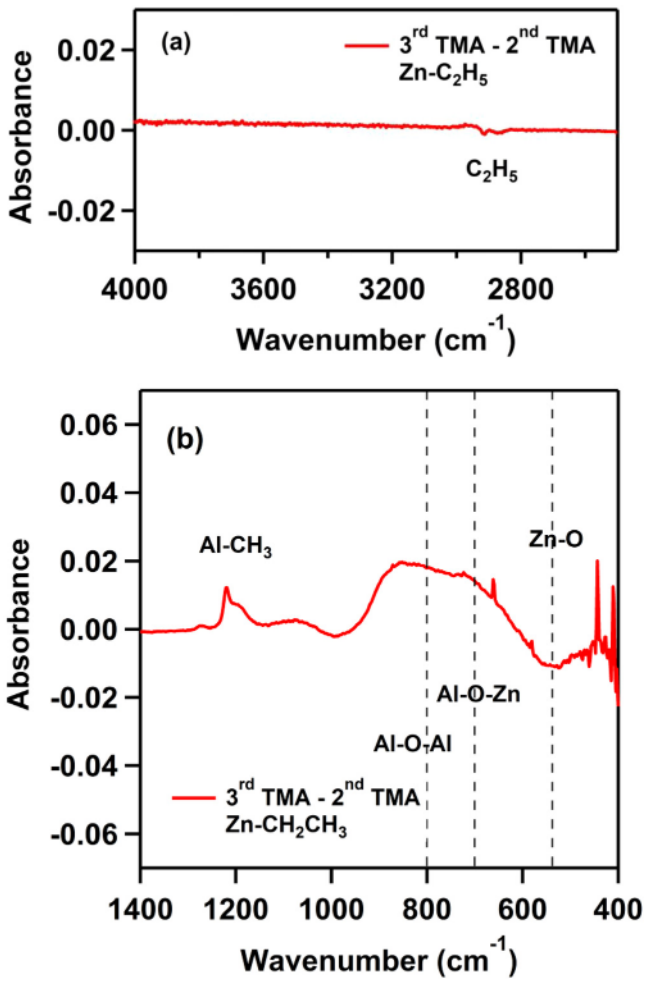

FIG. 12. FTIR difference spectrum showing the absorbance of (a) O–H and C–H stretching vibrations and (b) Al–O and Zn–O vibrational modes after the ethyl-terminated ZnO surface was exposed to the third TMA dose at 150 °C. The reference spectrum was obtained after the second TMA dose.

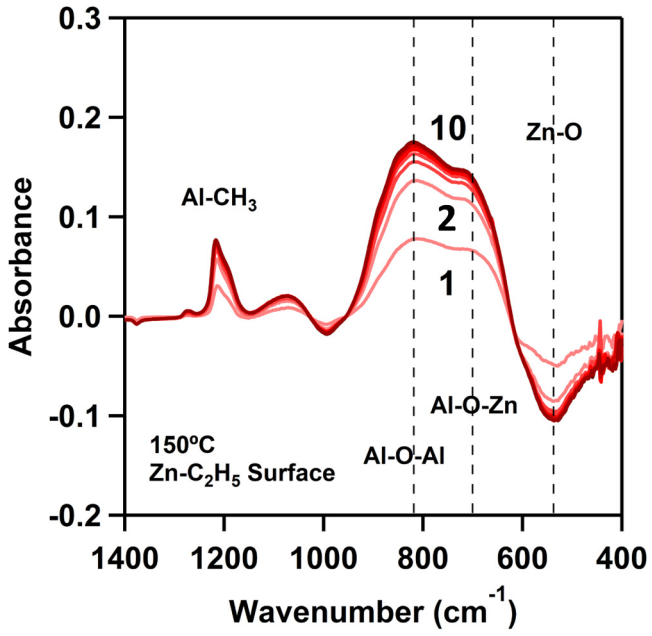

FIG. 13. FTIR difference spectra showing the absorbance of Al-O and Zn-O vibrational modes during consecutive TMA doses on an ethyl-terminated ZnO surface at 150 °C.

ZnO surface to produce ZnO-$Al(CH_3)_2$* species and gas phase CH_4.

Figure 14 shows the evolution of gaseous species during TMA exposures at 4 Torr onto the hydroxyl-terminated ZnO surfaces at 150 °C. The first TMA exposure yields a large amount of CH_4 at m/z = 16 as the primary reaction product. CH_4 is the expected reaction product from Eq. (8). There is also a small amount of $Zn(CH_3)_2$ [dimethylzinc (DMZ)] at m/z = 94, 76, and 64. The appearance of DMZ is consistent with some ZnO conversion to Al_2O_3 on the first TMA exposure as anticipated by Eq. (3).[9]

The gaseous products are very different during the second TMA exposure. Figure 14 shows a dramatic reduction of the CH_4 reaction product and an increase in the initial TMA reactant. In addition, the DMZ conversion product is much larger than during

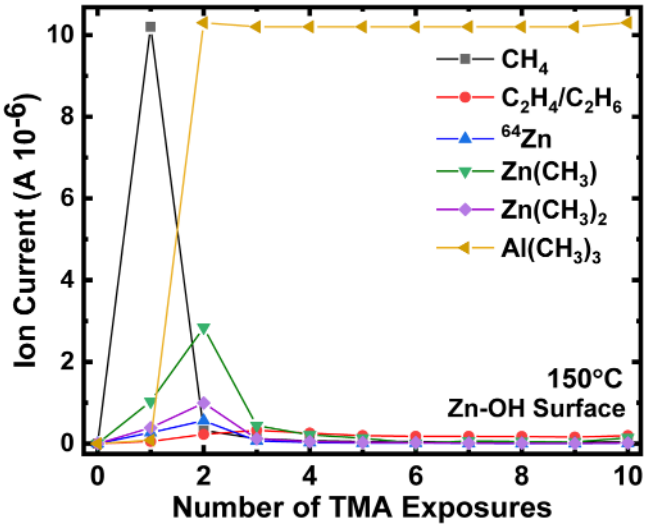

FIG. 14. Ion currents measured by mass spectrometry showing the evolution of gaseous reaction products during consecutive TMA exposures at 4 Torr on a hydroxyl-terminated ZnO surface at 150 °C.

the first TMA exposure. The growth of DMZ indicates that more conversion of ZnO to Al_2O_3 occurs after the initial reaction between TMA and the hydroxyl-terminated ZnO surface. The results for the subsequent TMA exposures reveal that the conversion reaction has saturated because only TMA is observed for larger numbers of TMA exposures.

TMA exposures were also performed on an ethyl-terminated ZnO surface at 150 °C. Figure 15 shows the evolution of the reaction products versus the number of TMA exposures at 4 Torr on the ethyl-terminated ZnO surface. The main products during the first TMA exposure are CH_4 at m/z = 16, C_2H_4 and/or C_2H_6 at m/z = 28, and a small amount of $Zn(CH_3)_2$ at m/z = 94, 76, and 64. The production of these reaction products suggests that the first TMA exposure may react with ZnC_2H_5* surface species according to

$$3OZnC_2H_5{}^*+4O^*+4Al(CH_3)_3 \rightarrow 3O_2AlCH_3{}^*+OAl(CH_3)_2{}^*+3Zn(CH_3)_2+2C_2H_4+C_2H_6+CH_4. \quad (11)$$

This reaction assumes that the ethyl ligands on ZnC_2H_5* species undergo β-hydride elimination to produce C_2H_4 and ZnH* species. The hydrogen ligands on ZnH* can then combine with either a methyl ligand from TMA to release CH_4 or with an ethyl ligand from ZnC_2H_5* to produce C_2H_6. Extra oxygen sites on the ZnO surface are also needed to bind the $Al(CH_3)_x$* species. This reaction is speculative but can explain the various mass spectrometry signals. The CH_4 mass signal in Fig. 15 is larger than expected given Eq. (11). Hydroxyl groups on the ethylated ZnO surface would produce additional CH_4. However, multiple $Zn(CH_2CH_3)_2$ exposures were employed to produce a fully ethylated ZnO surface.

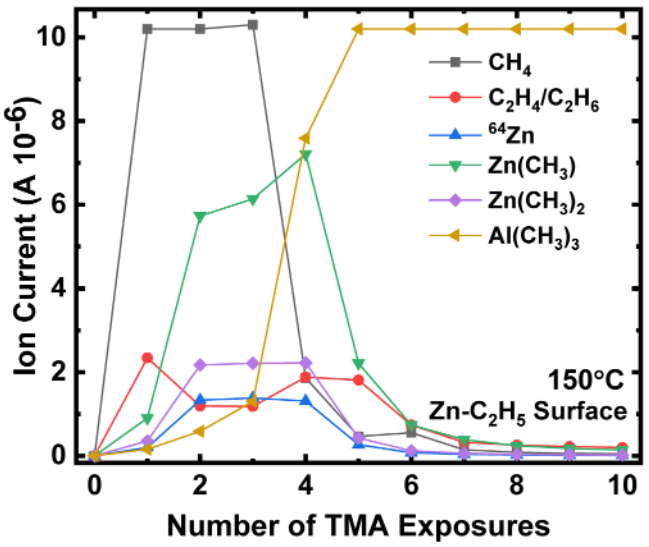

FIG. 15. Ion currents measured by mass spectrometry showing the evolution of gaseous reaction products during consecutive TMA exposures at 4 Torr on an ethyl-terminated ZnO surface at 150 °C.

During the second and third TMA exposures, Fig. 15 shows that CH_4 remains the main reaction product with DMZ progressively increasing relative to CH_4. The CH_4 signal intensity decreases dramatically during the fourth TMA exposure as DMZ becomes the main reaction product. DMZ then decreases and the TMA reactant is the main signal during the fifth DMZ exposure. This behavior indicates that most ZnO conversion to Al_2O_3 occurs during the second, third, and fourth TMA exposures. The ZnO conversion to Al_2O_3 is almost complete by the sixth TMA exposure.

The detection of DMZ with no evidence of $Zn(CH_2CH_3)(CH_3)$ (ethylmethylzinc) suggests that the ethyl-terminated species are removed prior to the ZnO to Al_2O_3 conversion reaction. A comparison of the ion currents in Figs. 14 and 15 reveals that the ZnO to Al_2O_3 conversion reaction by TMA on the ethylated ZnO surface produces more DMZ than the conversion reaction on the hydroxylated ZnO surface. This behavior may be explained by the different TMA reactions on ethyl-terminated and hydroxyl-terminated ZnO. On the hydroxyl-terminated ZnO, the TMA reacts with hydroxyl groups prior to the ZnO to Al_2O_3 conversion reaction. The resulting Zn-O-$Al(CH_3)_2$* species may then act as a partial barrier for the conversion reaction.

C. High TMA exposures

The previous FTIR and mass spectrometry results are consistent with the conversion of ZnO to Al_2O_3. In addition, these results indicate that the Al_2O_3 surface layer may act as a diffusion barrier that slows additional conversion. High exposure TMA experiments were performed to determine the extent of the conversion reaction. These experiments were performed on both ZnO nanoparticles and ZnO thin films on witness wafers. The TMA exposures ranged from 5 Torr s to 1200 Torr s.

XRR was utilized to measure the thickness of the Al_2O_3 surface layer on the ZnO thin film. Figure 16 shows XRR scans before and after a TMA exposure of 1200 Torr s. The Kiessig fringes of the original XRR scan before TMA exposures are further apart after the TMA exposure. The greater distance between the fringes corresponds to a thinner ZnO film. As illustrated in Fig. 17, the initial ZnO film thickness is 10.0 nm. The XRR scan after the TMA exposure displays features consistent with a thin Al_2O_3 layer with a thickness of 1.0 nm on the ZnO film. The thickness of the ZnO film is reduced to 8.2 nm.

ZnO conversion to Al_2O_3 also produces a mass reduction. According to Eq. (3), the conversion of ZnO to Al_2O_3 corresponds to a mass loss of 140.26 g/mol. This mass loss can be used as another measurement of ZnO to Al_2O_3 conversion. Mass loss experiments were conducted using ZnO nanoparticles with an initial diameter of 10 nm. Figure 18 shows the ZnO percent mass loss as a function of the number of TMA exposures at 1 Torr for 60 s. Measurements at 150 and 220 °C show self-limiting behavior for the conversion reaction. The percent mass loss reaches 49% for the highest TMA exposure of 1200 Torr s at 150 °C. These results are consistent with an Al_2O_3 conversion layer on the ZnO particles that acts as a diffusion barrier.

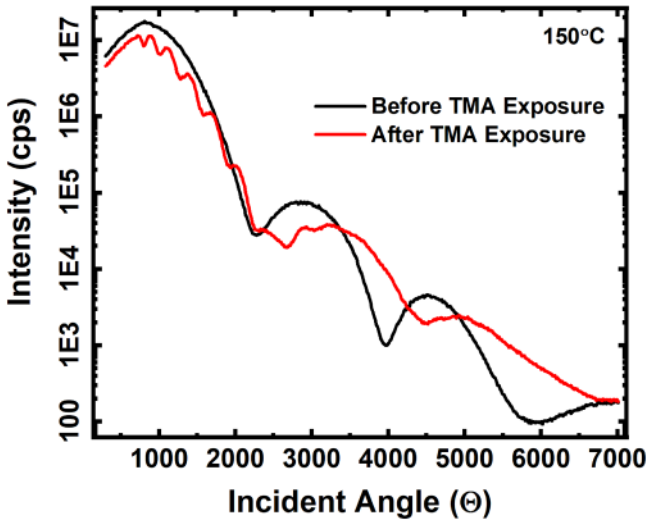

FIG. 16. XRR scans before and after TMA exposure of 1200 Torr s on a ZnO thin film with a thickness of 10.0 nm at 150 °C.

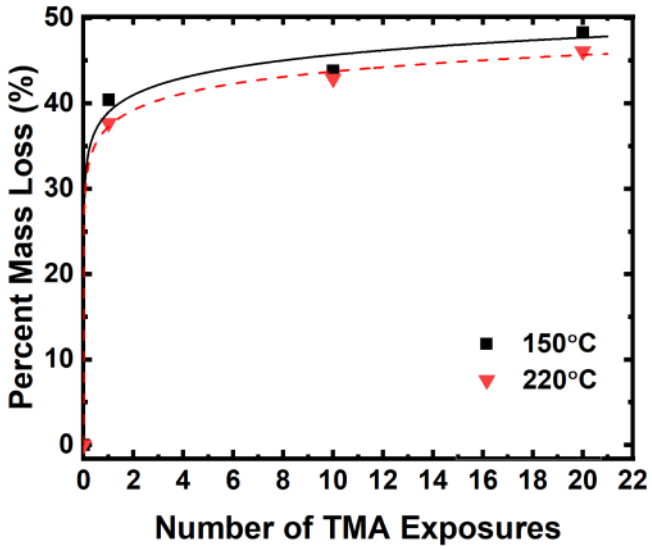

FIG. 18. Percent mass loss of ZnO nanoparticles with a diameter of 10.0 nm after TMA exposures of 60, 600, and 1200 Torr s at 150 and 220 °C.

A 49% mass loss for a ZnO particle with a 10 nm diameter corresponds to ZnO conversion to Al_2O_3 to yield an Al_2O_3 shell with a thickness of ~0.75 nm on the underlying ZnO particle. This Al_2O_3 thickness is smaller than the Al_2O_3 thickness of 1.0 nm observed by the XRR scans. However, this calculation only considers the ZnO conversion to Al_2O_3. The reactions of TMA with surface hydroxyl species are not included in this treatment. The reaction of TMA with surface hydroxyl species would increase the mass. Additional mass loss by ZnO to Al_2O_3 conversion would be needed to reach a mass loss of 49%. Therefore, the Al_2O_3 thickness on the ZnO nanoparticles may be closer to 1 nm. This TMA reaction with the hydroxyl-terminated ZnO nanoparticles would create

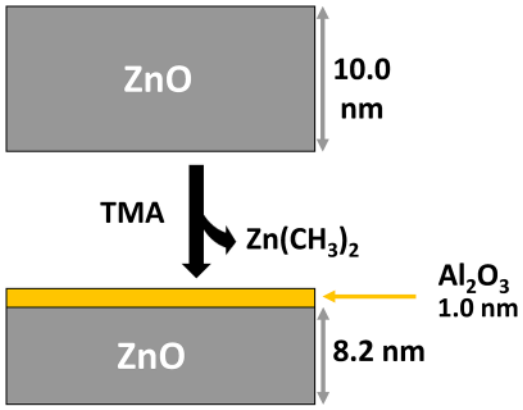

FIG. 17. Schematic showing an Al_2O_3 film with a thickness of 1.0 nm on top of a ZnO film as a result of ZnO conversion via TMA. Thicknesses were obtained by modeling XRR spectra before and after TMA exposure of 1200 Torr s.

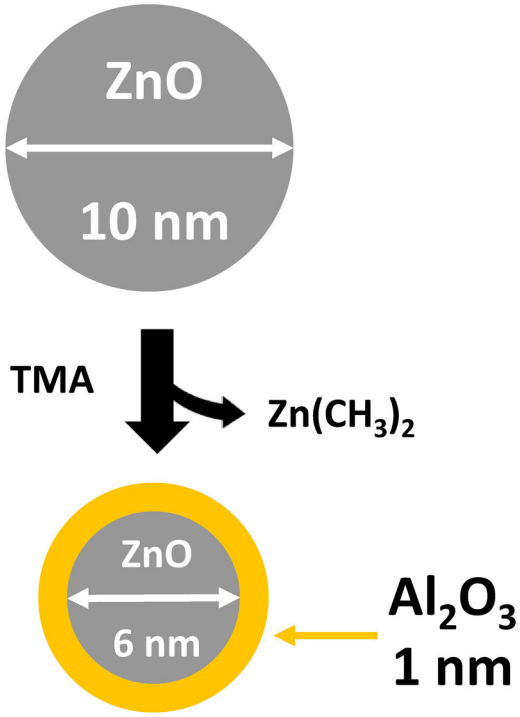

FIG. 19. Schematic of Al_2O_3/ZnO core–shell nanoparticle as a result of ZnO conversion via TMA. The mass loss of the ZnO nanoparticles observed in Fig. 18 is consistent with an Al_2O_3 shell with a thickness of 1.0 nm around the ZnO core particle.

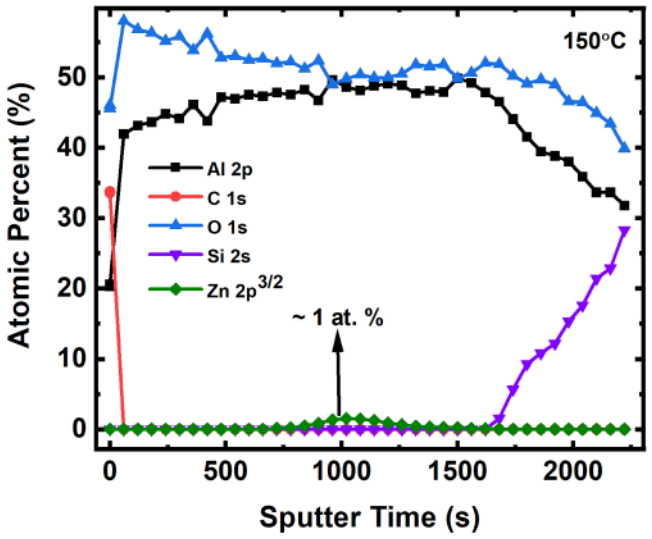

FIG. 20. XPS depth profile showing atomic percent vs sputter time for ZnO films with a thickness of 2.0 nm after TMA exposure of 1200 Torr s at 150 °C. The initial ZnO film is almost completely converted to Al_2O_3.

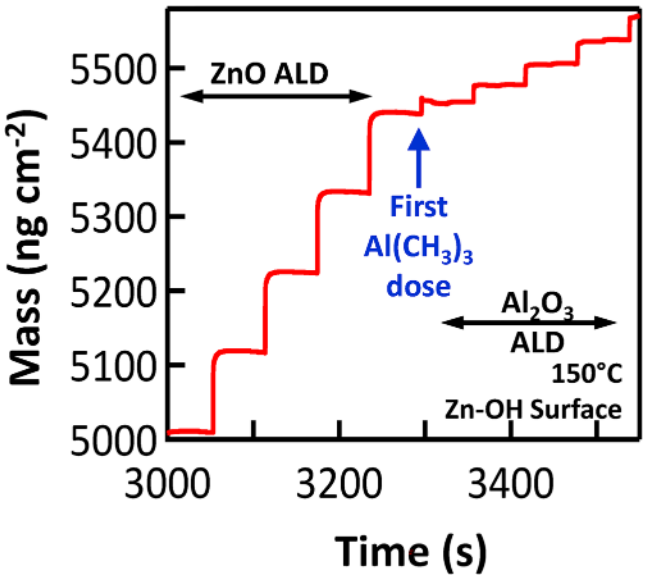

FIG. 21. QCM measurements of mass vs time showing ZnO ALD and then Al_2O_3 ALD at 150 °C. The arrow highlights the mass gain during the first TMA exposure on a hydroxyl-terminated ZnO surface after 50 cycles of ZnO ALD.

a core–shell composite with an Al_2O_3 shell on a ZnO core, as depicted in Fig. 19.

The extent of ZnO conversion to Al_2O_3 can also be measured using XPS depth profiling. Experiments were performed on an initial ZnO ALD film with a thickness of 2.0 nm on a silicon wafer. This ZnO film was then exposed to a TMA exposure of 1200 Torr s at 150 °C. Figure 20 shows the XPS depth-profiling results for this film. The XPS results are consistent with an almost complete conversion of the ZnO thin film to Al_2O_3. The profile shows Al and O in the film with a negligible amount of Zn at ~1.5 at% deep in the film. The absence of Zn in the film is expected from ZnO to Al_2O_3 conversion. The XRR measurements were consistent with 1.0 nm of Al_2O_3 added for each 1.8 nm of ZnO lost during conversion. The almost complete conversion of the ZnO film with an initial thickness of 2.0 nm is in agreement with the previous XRR results.

D. Quartz crystal microbalance measurements

The conversion of ZnO to Al_2O_3 can also be observed by QCM measurements. As discussed earlier, QCM studies of ZnO/Al_2O_3 nanolaminate growth were the first to document the reaction of TMA with ZnO.[8] Additional experiments of ZnO/Al_2O_3 nanolaminate growth were performed in the current study to evaluate the TMA reaction with hydroxyl-terminated or ethyl-terminated ZnO surfaces. Compared with the high TMA exposure studies, these QCM experiments were conducted at lower TMA exposures of 0.8–0.9 Torr s.

Figure 21 depicts QCM measurements highlighting the first TMA exposure on a ZnO ALD film with a thickness of 10 nm grown using 50 cycles ZnO ALD cycles. This ZnO ALD film was terminated with hydroxyl groups remaining after the last H_2O exposure during ZnO ALD. The first TMA exposure during Al_2O_3 ALD at 150 °C leads to a small mass gain of about 12 ng/cm^2. The mass loss expected for the conversion reaction is not dominant

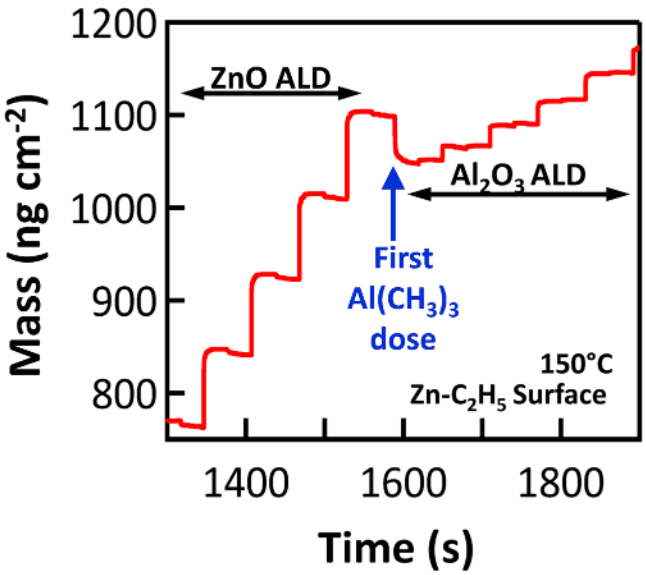

FIG. 22. QCM measurements of mass vs time showing ZnO ALD and then Al_2O_3 ALD at 150 °C. The arrow highlights the mass loss during the first TMA exposure on an ethyl-terminated ZnO surface after 50 cycles of ZnO ALD.

because TMA adds mass by reacting with the hydroxyl groups and masks the conversion reaction.

To eliminate the reaction of TMA with hydroxyl species, the ZnO ALD during ZnO/Al_2O_3 nanolaminate growth was stopped after the DEZ exposure. This procedure leaves an ethyl-terminated ZnO surface. Figure 22 shows the QCM measurements highlighting TMA exposure to an ethyl-terminated ZnO surface at 150 °C. This TMA exposure leads to a large mass loss of approximately 50 ng/cm^2. Without the competing reaction of TMA with hydroxyl groups on ZnO, the ZnO to Al_2O_3 conversion reaction produces a pronounced mass loss. Previous QCM studies have also explored TMA exposures on ethyl-terminated ZnO surfaces during the growth of Al-doped ZnO.[59]

QCM measurements were then conducted for various ZnO/Al_2O_3 nanolaminates grown using sequences of x ZnO ALD cycles and x Al_2O_3 ALD cycles. Figure 23 shows mass changes after the first TMA exposure on both hydroxyl-terminated and ethyl-terminated ZnO surfaces when growing the ZnO/Al_2O_3 nanolaminate using sequences of x ZnO ALD cycles and x Al_2O_3 ALD cycles. The mass loss on the ethyl-terminated ZnO surface is much larger than the mass loss on the hydroxyl-terminated ZnO surface. The difference in the mass loss between the ethyl-terminated and hydroxyl-terminated surfaces is relatively constant at about 95–100 ng/cm^2 for the various x values.

There are also changes in the mass loss versus x in the sequences of x ZnO ALD cycles and x Al_2O_3 ALD cycles. The mass losses increase versus x, reach a maximum at x = 6–8, and then decrease for larger x before leveling off at x > 25–30. These changes in mass loss versus x may be explained by the nucleation of ZnO ALD on the Al_2O_3 surface. The initial ZnO films on the Al_2O_3 surface may be easier to convert than the thicker ZnO films. Perhaps the initial ZnO films are more amorphous and the amorphous structure facilitates conversion to Al_2O_3. The thicker ZnO films become crystalline and may be harder to convert to Al_2O_3 at x > 15.

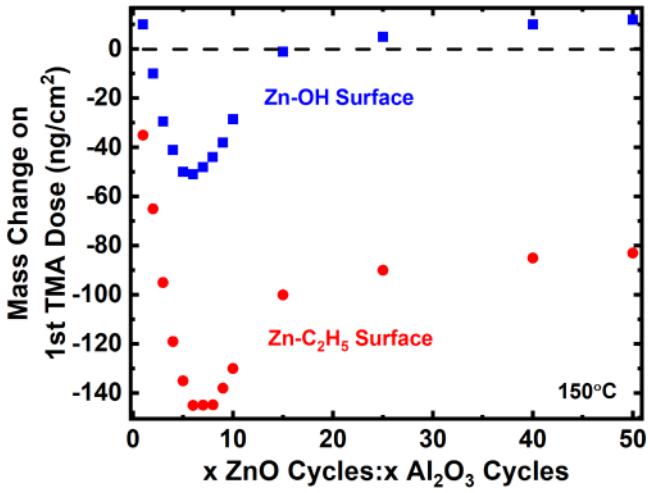

FIG. 23. QCM measurement of mass changes after the first TMA exposure at 150 °C on hydroxyl-terminated and ethyl-terminated ZnO surfaces. Mass changes were obtained when growing ZnO/Al_2O_3 nanolaminates using a sequence of x ZnO ALD cycles and x Al_2O_3 ALD cycles.

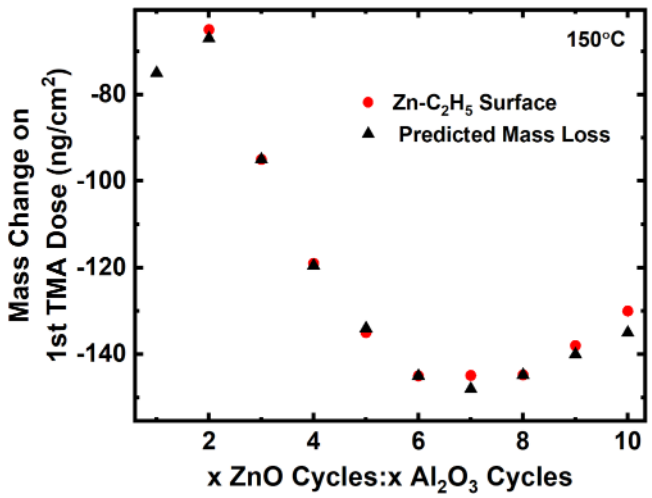

FIG. 24. Comparison between predicted mass loss and mass change on an ethyl-terminated ZnO surface after the first TMA exposure when growing ZnO/Al_2O_3 nanolaminates using a sequence of x ZnO ALD cycles and x Al_2O_3 ALD cycles.

The mass change for the ethyl-terminated ZnO surfaces is 95–100 ng/cm^2 more negative than the mass change for the hydroxyl-terminated ZnO surfaces. The larger mass loss during the TMA exposures on the ethyl-terminated ZnO surface can be

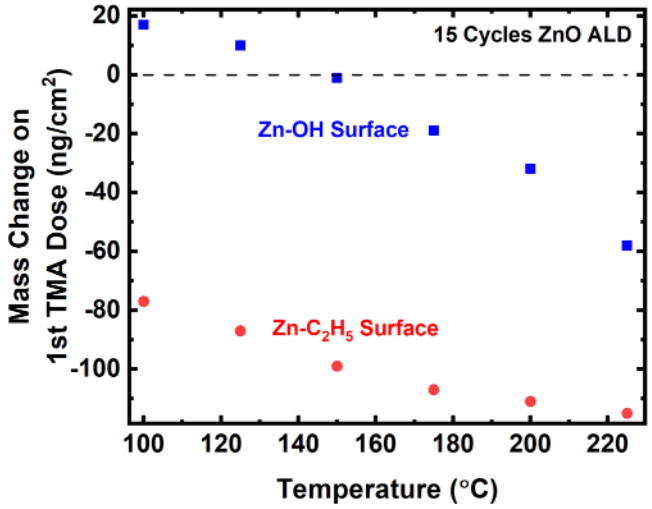

FIG. 25. Temperature dependence of mass changes after first TMA exposure on hydroxyl-terminated and ethyl-terminated ZnO surfaces grown with 15 cycles of ZnO ALD.

partially attributed to the loss of the ethyl groups on the ethyl-terminated ZnO surface. The loss of these ethyl groups was confirmed by the FTIR studies. The smaller mass loss during the TMA exposures on the hydroxyl-terminated ZnO surface is also explained by the reaction of TMA with the hydroxyl groups. This reaction adds ZnO-Al$(CH_3)_x$* species to the surface and offsets the mass loss caused by conversion.

Figure 24 shows the measured mass changes after the first TMA exposure on the ethyl-terminated ZnO surfaces versus x in the sequences of x ZnO ALD cycles and x Al_2O_3 ALD cycles. In comparison, the predicted mass loss is also shown based on a model that assumes that all the Zn and ethyl groups from the previous DEZ exposure during ZnO ALD leave as DMZ, C_2H_6, and C_2H_4. In addition, the remaining ZnO after removing the Zn

TABLE I. Conversion reactions of various metal oxides. Reference 40 is used to perform thermochemical calculations of standard free energy change.

Conversion reactions of various metal oxides		
Conversion reaction	ΔG(150 °C) (kcal/mol)	Reference
1. Trimethylaluminum—$Al(CH_3)_3$		
$As_2O_3 + 2Al(CH_3)_3 \rightarrow Al_2O_3 + 2As(CH_3)_3$		18, 20, 21, 23, 61–63
$Ga_2O_3 + 2Al(CH_3)_3 \rightarrow Al_2O_3 + 2Ga(CH_3)_3$		18, 20, 21, 23
$In_2O_3 + 2Al(CH_3)_3 \rightarrow Al_2O_3 + 2In(CH_3)_3$	−318	40, 64
$3SiO_2 + 4Al(CH_3)_3 \rightarrow 2Al_2O_3 + 3Si(CH_3)_4$	−200	28, 40
$3SnO_2 + 4Al(CH_3)_3 \rightarrow 2Al_2O_3 + 3Sn(CH_3)_4$	−229	40
$3ZnO + 2Al(CH_3)_3 \rightarrow Al_2O_3 + 3Zn(CH_3)_3$	−165	9, 26, 40
$Sb_2O_3 + Al(CH_3)_3 \rightarrow Al_2O_3 + Sb(CH_3)_3$		64
2. Tetrakis(ethylmethylamino)hafnium—$Hf[NCH_3C_2H_5]_4$ (or Tetrakis(dimethylamino)hafnium)		
$2As_2O_3 + 3Hf[NCH_3C_2H_5]_4 \rightarrow 3HfO_2 + 4As[NCH_3C_2H_5]_4$		17–19, 22, 65, 66
$2Ga_2O_3 + 3Hf[NCH_3C_2H_5]_4 \rightarrow 3HfO_2 + 4Ga[NCH_3C_2H_5]_4$		17–19, 22, 65
$2In_2O_3 + 3Hf[NCH_3C_2H_5]_4 \rightarrow 3HfO_2 + 4In[NCH_3C_2H_5]_4$		17, 19, 65, 66
3. Titanium tetrachloride—$TiCl_4$		
$As_2O_3 + 3/2TiCl_4 \rightarrow 3/2TiO_2 + 2AsCl_3$	−42	40
$CrO_3 + 1/2TiCl_4 \rightarrow 1/2TiO_2 + CrO_2Cl_2$	−18	40
$Fe_2O_3 + 3/2TiCl_4 \rightarrow 3/2TiO_2 + 2FeCl_3$	−3	40
$GeO_2 + TiCl_4 \rightarrow TiO_2 + GeCl_4$	−22	40
$MoO_3 + 1/2TiCl_4 \rightarrow 1/2TiO_2 + MoO_2Cl_2$	−25	40
$Sb_2O_3 + 3/2TiCl_4 \rightarrow 3/2TiO_2 + 2SbCl_3$	−6	40
$SnO_2 + TiCl_4 \rightarrow TiO_2 + SnCl_4$	−54	40
$As_2O_3 + 3/2TiCl_4 \rightarrow 3/2TiO_2 + 2AsCl_3$	−21	40
4. Boron trichloride—BCl_3		
$As_2O_3 + 2BCl_3 \rightarrow B_2O_3 + 2AsCl_3$	−81	40
$Au_2O_3 + 2BCl_3 \rightarrow B_2O_3 + 2AuCl_3$	−135	40
$CrO_3 + 2/3BCl_3 \rightarrow 1/3B_2O_3 + CrO_2Cl_2$	−94	40
$Fe_2O_3 + 2BCl_3 \rightarrow B_2O_3 + 2FeCl_3$	−42	40
$Ga_2O_3 + 2BCl_3 \rightarrow B_2O_3 + 2GaCl_3$	−62	40
$GeO_2 + 4/3BCl_3 \rightarrow 2/3B_2O_3 + GeCl_4$	−77	40
$HfO_2 + 4/3BCl_3 \rightarrow 2/3B_2O_3 + HfCl_4$	−16	40
$MoO_3 + 2/3BCl_3 \rightarrow 1/3B_2O_3 + MoO_2Cl_2$	−19	40
$NbO_2 + 4/3BCl_3 \rightarrow 2/3B_2O_3 + NbCl_4$	−14	40
$Sb_2O_3 + 2BCl_3 \rightarrow B_2O_3 + 2SbCl_3$	−94	40
$Ta_2O_5 + 10/3BCl_3 \rightarrow 5/3B_2O_3 + 2TaCl_5$	−43	40
$VO_2 + 4/3BCl_3 \rightarrow 2/3B_2O_3 + VCl_4$	−26	40
$V_2O_5 + 2BCl_3 \rightarrow B_2O_3 + VOCl_3$	−67	40
$WO_3 + 2BCl_3 \rightarrow B_2O_3 + WCl_6$	−10	31, 40
$ZrO_2 + 4/3BCl_3 \rightarrow 2/3B_2O_3 + ZrCl_4$	−16	40
5. Trimethylborane—$B(CH_3)_3$		
$As_2O_3 + 2B(CH_3)_3 \rightarrow B_2O_3 + 2As(CH_3)_3$	−83	40
$GeO_2 + 4/3B(CH_3)_3 \rightarrow 2/3B_2O_3 + Ge(CH_3)_4$	−46	40
$In_2O_3 + 2B(CH_3)_3 \rightarrow B_2O_3 + 2In(CH_3)_3$	−127	40
$SnO_2 + 4/3B(CH_3)_3 \rightarrow 2/3B_2O_3 + Sn(CH_3)_4$	−27	40

and ethyl groups from the previous DEZ exposure was assumed to behave similar to a hydroxylated ZnO film after x−1 ZnO ALD cycles.

The following example illustrates this prediction. Figure 24 shows a mass loss of 145 ng/cm^2 at x = 6 during the first TMA exposure on the ethyl-terminated surface. The mass gain of 95 ng/cm^2 from the previous DEZ exposure during ZnO ALD is assumed to be lost during the first TMA exposure. ZnO is assumed to be converted to Al_2O_3 by TMA according to the results for the first TMA exposure on the hydroxyl-terminated ZnO surface at x−1 = 5 ZnO ALD cycles. Experiments on the hydroxyl-terminated ZnO surface yielded a mass loss of 50 ng/cm^2 for the first TMA exposure at x−1 = 5. The loss of the 95 ng/cm^2 mass gain from the previous DEZ exposure, together with the mass loss of 50 ng/cm^2, yields a total mass loss of 145 ng/cm^2. This total predicted mass loss of 145 ng/cm^2 is in excellent agreement with the 145 ng/cm^2 mass loss measured at x = 6 in Fig. 24.

This model was used to predict the mass change versus x for the other x values in Fig. 24. There is excellent agreement between the measured mass lost and the predicted mass loss for all the x values. The differences start to become noticeable at x > 6. However, the differences are never more than 10 ng/cm^2. This agreement supports the mechanism where TMA exposures on the ethyl-terminated ZnO surface lead to the loss of Zn and ethyl groups from the previous DEZ exposure during ZnO ALD. Subsequently, the TMA converts the remaining ZnO to Al_2O_3 similar to TMA on a hydroxyl-terminated ZnO surface.

The temperature dependence of the ZnO conversion to Al_2O_3 by TMA was also observed for the hydroxyl-terminated and ethyl-terminated ZnO surfaces. Figure 25 shows the mass change after the first TMA exposure on both a hydroxylated and ethylated ZnO surface at various temperatures following 15 cycles of ZnO ALD. The mass changes are compared after 15 cycles of ZnO ALD, because Fig. 23 shows that the mass changes start to level out versus x at x = 15. Figure 25 reveals that higher temperatures lead to a greater conversion of ZnO to Al_2O_3.

The mass changes become increasingly negative for both hydroxyl-terminated and ethyl-terminated surfaces at higher temperatures. The increase in mass change is less for the ethyl-terminated ZnO surface at higher temperatures. This behavior may reflect the limiting nature of the ZnO to Al_2O_3 conversion reaction. Because the ethyl-terminated ZnO surface has converted more to Al_2O_3 at lower temperatures, the ethyl-terminated ZnO surface allows less additional conversion of ZnO to Al_2O_3 at higher temperatures. In contrast, very little temperature dependence was observed for the percent mass loss measurements in Fig. 18 for Zn nanoparticles after much higher TMA exposures. These higher TMA exposures were able to reach the saturation limit for the conversion reaction at the two temperatures investigated in Fig. 18.

V. GENERALITY OF CONVERSION REACTIONS

Conversion reactions in atomic layer processing are expected to be ubiquitous if the reactions are thermochemically favorable and the reaction products are volatile. The appreciation of conversion reactions is not widely acknowledged because the conversion can be limited to very thin thicknesses. These thicknesses may be negligible relative to the thickness of the deposited ALD film. However, during the growth of ALD alloys or layered structures based on alternating ALD cycles, the consequence of conversion reactions can be considerable.[7,8] In addition, the effects of conversion reactions cannot be ignored as atomic layer processing continues to demand thinner films.

Using metal oxides as an example, the observation of conversion should be very likely if the metal oxide being formed is thermodynamically favored compared with the original metal oxide on the surface. This generality assumes that the metal in the original metal oxide is stable and volatile with the ligands from the incoming metal precursor. Table I lists various conversion reactions for several metal precursors. These reactions have either been implied by results in the literature or predicted based on thermochemical calculations.[40] Other reactions may also compete with these conversion reactions. For example, $TiCl_4$ may react with As_2O_3 to produce gaseous $TiOCl_2$ and AsCl.[23] There is also evidence that TDMA-Hf may remove native oxides on InAs surfaces by an etching process prior to forming HfO_2.[60]

Although conversion reactions are a complication, they can provide many benefits. The "self-cleaning" of the oxides from GaAs surfaces is one prominent example of the value of conversion reactions.[18,20,22,23] Another example is conversion reactions in thermal ALE that allow some materials to be etched that are not etched using other etching mechanisms.[28–31] Conversion reactions should be actively considered as a strategy in atomic layer processing. Conversion should become a tool by which materials can be transformed to be compatible with the subsequent processing step or to achieve the desired structure.

VI. CONCLUSIONS

This perspective has reviewed conversion reactions in atomic layer processing including ALD and ALE. These conversion reactions may involve the exchange of either the metal cation or the oxygen or sulfur anion in the thin film. If the conversion reactions are thermochemically possible, then they should be considered a viable possibility. However, these conversions may not be fully appreciated because they may self-limit at the Ångstrom level. Although these exchange processes may be ubiquitous, only a few experimental and theoretical results at the atomic scale have recognized their importance.

The perspective first reviewed some key previous examples of exchange processes, including ZnO conversion to Al_2O_3 by TMA, cleaning of GaAs surfaces by TMA and TEMA–Hf or TDMA–Hf, and ZnO conversion to ZnS by H_2S. The paper then focused in detail on the conversion of ZnO to Al_2O_3 by TMA. This model conversion reaction was documented using a variety of techniques, including FTIR spectroscopy, quadrupole mass spectrometry (QMS), x-ray reflectivity (XRR), gravimetric analysis, x-ray photoelectron spectroscopy (XPS), and quartz crystal microbalance (QCM) measurements. These techniques all revealed different signatures of ZnO conversion to Al_2O_3 using TMA.

The FTIR spectroscopy, QMS, and XPS studies confirmed the conversion reaction as $3ZnO + 2Al(CH_3)_3(g) \rightarrow Al_2O_3 + 3Zn(CH_3)_2(g)$. The FTIR studies determined that the conversion

reaction continues to proceed after completion of the initial surface reaction. The QMS investigations revealed that the initial TMA exposures yielded CH_4 as a reaction product from both hydroxyl-terminated and ethyl-terminated ZnO surfaces. The appearance of CH_4 and C_2H_4/C_2H_6 from the ethyl-terminated ZnO surfaces suggested that the $ZnCH_2CH_3$* species undergo β-hydride elimination to produce C_2H_4 followed by H transfer from ZnH* species to produce CH_4 and C_2H_6 from TMA and $ZnCH_2CH_3$*, respectively. The XRR investigations, gravimetric analysis, and XPS measurements established that the Al_2O_3 film formed on ZnO resulting from conversion after large TMA exposures at 150 °C had a film thickness of approximately 1 nm. The Al_2O_3 film thickness was similar on flat ZnO films on silicon wafers and ZnO nanoparticles.

The conversion occurred for both hydroxyl-terminated and ethyl-terminated ZnO surfaces. The QCM studies revealed that the mass changes were different for the hydroxyl-terminated and ethyl-terminated ZnO surfaces. The difference was explained by the reaction of TMA with the hydroxyl surface species on ZnO in addition to the conversion reaction. The mass loss for the ethyl-terminated ZnO surface was accurately predicted by assuming that the TMA removes the Zn and ethyl groups from the previous DEZ exposure and then converts the ZnO surface similar to TMA on a hydroxylated ZnO surface. Although the conversion reaction was self-limiting using higher TMA exposures, temperature-dependent QCM studies at lower TMA exposures revealed that higher temperatures led to more conversion.

Conversion reactions should be expected during ALD and thermal ALE processing. Conversion reactions are expected to be most noticeable during the nucleation of ALD processes. Conversion may also be very useful for cleaning surfaces or for converting one material that may not easily etch into a different material that may have accessible etching pathways. Many other possible applications of conversion reactions in areas such as area selective deposition or area selective etching are likely. Conversion should be considered as a tool to expand the possibilities for atomic layer processing.

ACKNOWLEDGMENTS

The experimental work on ZnO conversion to Al_2O_3 by trimethylaluminum reported in this paper was supported by the National Science Foundation (NSF) (x-ray reflectivity, gravimetric analysis, and x-ray photoelectron spectroscopy), Intel Corporation through a member-directed grant administered by the Semiconductor Research Corporation (FTIR spectroscopy), Lam Research (mass spectrometry), and the Department of Energy (quartz crystal microbalance measurements). The authors thank Gordana Dukovic and Leah Hall in the Department of Chemistry at the University of Colorado at Boulder for help preparing the ZnO nanoparticles. The authors also thank Andrew S. Cavanagh for obtaining the x-ray photoelectron spectroscopy results.

DATA AVAILABILITY

The data that support the findings of this study are available within the article.

REFERENCES

[1]S. M. George, Chem. Rev. **110**, 111 (2010).
[2]S. M. George, Acc. Chem. Res. **53**, 1151 (2020).
[3]R. L. Puurunen, J. Appl. Phys. **97**, 121301 (2005).
[4]S. Klejna and S. D. Elliott, J. Phys. Chem. C **116**, 643 (2012).
[5]S. Klejna and S. D. Elliott, Chem. Mater. **26**, 2427 (2014).
[6]L. Lamagna, C. Wiemer, M. Perego, S. Spiga, J. Rodriguez, D. S. Coll, M. E. Grillo, S. Klejna, and S. D. Elliott, Chem. Mater. **24**, 1080 (2012).
[7]A. J. M. Mackus, J. R. Schneider, C. MacIsaac, J. G. Baker, and S. F. Bent, Chem. Mater. **31**, 1142 (2019).
[8]J. W. Elam and S. M. George, Chem. Mater. **15**, 1020 (2003).
[9]J. W. Elam, J. A. Libera, M. J. Pellin, and P. C. Stair, Appl. Phys. Lett. **91**, 243105 (2007).
[10]J. M. Lee, K. M. Chang, K. K. Kim, W. K. Choi, and S. J. Park, J. Electrochem. Soc. **148**, G1 (2001).
[11]P. Genevee, F. Donsanti, G. Renou, and D. Lincot, J. Phys. Chem. C **115**, 17197 (2011).
[12]P. Genevee, F. Donsanti, N. Schneider, and D. Lincot, J. Vac. Sci. Technol. A **31**, 01a131 (2013).
[13]E. Thimsen, Q. Peng, A. B. F. Martinson, M. J. Pellin, and J. W. Elam, Chem. Mater. **23**, 4411 (2011).
[14]D. K. Lancaster, H. Sun, and S. M. George, J. Phys. Chem. C **121**, 18643 (2017).
[15]J. R. Bakke, J. T. Tanskanen, C. Haegglund, T. A. Pakkanen, and S. F. Bent, J. Vac. Sci. Technol. A **30**, 01a135 (2012).
[16]C. Platzer-Bjorkman, T. Torndahl, D. Abou-Ras, J. Malmstrom, J. Kessler, and L. Stolt, J. Appl. Phys. **100**, 044506 (2006).
[17]C. L. Hinkle, E. M. Vogel, P. D. Ye, and R. M. Wallace, Curr. Opin. Solid State Mater. Sci. **15**, 188 (2011).
[18]C. L. Hinkle *et al.*, Appl. Phys. Lett. **92**, 071901 (2008).
[19]C. H. Chang, Y. K. Chiou, Y. C. Chang, K. Y. Lee, T. D. Lin, T. B. Wu, M. Hong, and J. Kwo, Appl. Phys. Lett. **89**, 242911 (2006).
[20]J. Gao, G. He, S. Liang, D. Wang, and B. Yang, J. Mater. Chem. C **6**, 2546 (2018).
[21]M. Tallarida, C. Adelmann, A. Delabie, S. Van Elshocht, M. Caymax, and D. Schmeisser, Appl. Phys. Lett. **99**, 042906 (2011).
[22]R. Suri, D. J. Lichtenwalner, and V. Misra, Appl. Phys. Lett. **96**, 112905 (2010).
[23]B. Granados-Alpizar and A. J. Muscat, Surf. Sci. **605**, 1243 (2011).
[24]S. M. George and Y. Lee, ACS Nano **10**, 4889 (2016).
[25]Y. Lee and S. M. George, ACS Nano **9**, 2061 (2015).
[26]D. R. Zywotko and S. M. George, Chem. Mater. **29**, 1183 (2017).
[27]Y. Lee, C. Huffman, and S. M. George, Chem. Mater. **28**, 7657 (2016).
[28]J. W. DuMont, A. E. Marquardt, A. M. Cano, and S. M. George, ACS Appl. Mater. Interfaces **9**, 10296 (2017).
[29]A. I. Abdulagatov and S. M. George, Chem. Mater. **30**, 8465 (2018).
[30]A. I. Abdulagatov and S. M. George, J. Vac. Sci. Technol. A **38**, 022607 (2020).
[31]N. R. Johnson and S. M. George, ACS Appl. Mater. Interfaces **9**, 34435 (2017).
[32]J. W. DuMont and S. M. George, J. Phys. Chem. C **119**, 14603 (2015).
[33]J. D. Ferguson, A. W. Weimer, and S. M. George, J. Vac. Sci. Technol. A **23**, 118 (2005).
[34]J. W. Clancey, A. S. Cavanagh, J. E. T. Smith, S. Sharma, and S. M. George, J. Phys. Chem. C **124**, 287 (2020).
[35]J. A. McCormick, B. L. Cloutier, A. W. Weimer, and S. M. George, J. Vac. Sci. Technol. A **25**, 67 (2007).
[36]M. Moroni, D. Borrini, L. Calamai, and L. Dei, J. Colloid Interface Sci. **286**, 543 (2005).
[37]J. W. Elam, M. D. Groner, and S. M. George, Rev. Sci. Instrum. **73**, 2981 (2002).
[38]J. W. Elam, Z. A. Sechrist, and S. M. George, Thin Solid Films **414**, 43 (2002).
[39]Y. Lee, J. W. DuMont, and S. M. George, Chem. Mater. **28**, 2994 (2016).
[40]HSC Chemistry, *HSC Chemistry 5.1* (Outokumpu Research Oy, Pori).
[41]A. W. Ott, J. W. Klaus, J. M. Johnson, and S. M. George, Thin Solid Films **292**, 135 (1997).
[42]T. Tynell and M. Karppinen, Semicond. Sci. Technol. **29**, 043001 (2014).

[43]T. Minami, Semicond. Sci. Technol. **20**, S35 (2005).
[44]P. Banerjee, W.-J. Lee, K.-R. Bae, S. B. Lee, and G. W. Rubloff, J. Appl. Phys. **108**, 043504 (2010).
[45]N. P. Dasgupta, S. Neubert, W. Lee, O. Trejo, J.-R. Lee, and F. B. Prinz, Chem. Mater. **22**, 4769 (2010).
[46]J. W. Elam, D. Routkevitch, and S. M. George, J. Electrochem. Soc. **150**, G339 (2003).
[47]Y. Geng, L. Guo, S.-S. Xu, Q.-Q. Sun, S.-J. Ding, H.-L. Lu, and D. W. Zhang, J. Phys. Chem. C **115**, 12317 (2011).
[48]D. J. Lee, H. M. Kim, J. Y. Kwon, H. Choi, S. H. Kim, and K. B. Kim, Adv. Funct. Mater. **21**, 448 (2011).
[49]A. Abou Chaaya, R. Viter, I. Baleviciute, M. Bechelany, A. Ramanavicius, Z. Gertnere, D. Erts, V. Smyntyna, and P. Miele, J. Phys. Chem. C **118**, 3811 (2014).
[50]J. M. Jensen, A. B. Oelkers, R. Toivola, D. C. Johnson, J. W. Elam, and S. M. George, Chem. Mater. **14**, 2276 (2002).
[51]R. J. Collins and D. A. Kleinman, J. Phys. Chem. Solids **11**, 190 (1959).
[52]A. Kolodziejczak-Radzimska, E. Markiewicz, and T. Jesionowski, J. Nanomater. **2012**, 656353 (2012).
[53]S. C. Singh and R. Gopal, Phys. E Low Dimens. Syst. Nanostruct. **40**, 724 (2008).
[54]J. D. Ferguson, A. W. Weimer, and S. M. George, Chem. Mater. **16**, 5602 (2004).
[55]A. Boumaza, L. Favaro, J. Ledion, G. Sattonnay, J. B. Brubach, P. Berthet, A. M. Huntz, P. Roy, and R. Tetot, J. Solid State Chem. **182**, 1171 (2009).
[56]D. L. Ge, Y. J. Fan, C. L. Qi, and Z. X. Sun, J. Mater. Chem. A **1**, 1651 (2013).
[57]D. N. Goldstein, J. A. McCormick, and S. M. George, J. Phys. Chem. C **112**, 19530 (2008).
[58]B. E. Deal and A. S. Grove, J. Appl. Phys. **36**, 3770 (1965).
[59]J. S. Na, Q. Peng, G. Scarel, and G. N. Parsons, Chem. Mater. **21**, 5585 (2009).
[60]R. Timm *et al.*, Nat. Commun. **9**, 1412 (2018).
[61]A. P. Kirk, M. Milojevic, J. Kim, and R. M. Wallace, Appl. Phys. Lett. **96**, 202905 (2010).
[62]M. Milojevic, C. L. Hinkle, F. S. Aguirre-Tostado, H. C. Kim, E. M. Vogel, J. Kim, and R. M. Wallace, Appl. Phys. Lett. **93**, 252905 (2008).
[63]M. L. Huang, Y. C. Chang, C. H. Chang, Y. J. Lee, P. Chang, J. Kwo, T. B. Wu, and M. Hong, Appl. Phys. Lett. **87**, 252104 (2005).
[64]C. H. Hou, M. C. Chen, C. H. Chang, T. B. Wu, C. D. Chiang, and J. J. Luo, J. Electrochem. Soc. **155**, G180 (2008).
[65]Y. C. Chang *et al.*, Appl. Phys. Lett. **92**, 072901 (2008).
[66]R. Timm, A. Fian, M. Hjort, C. Thelander, E. Lind, J. N. Andersen, L. E. Wernersson, and A. Mikkelsen, Appl. Phys. Lett. **97**, 132904 (2010).